Variance in Orca Basin compound-specific GDGT $\delta^{13}C$: Implications for source, sink, and paleoclimate interpretations

Samantha Lichtin

Mark Pagani, Pincelli Hull

May 10, 2016

A Senior Thesis presented to the faculty of the Department of Geology and Geophysics, Yale University, in partial fulfillment of the Bachelor's Degree.

CONTENTS

INDEX OF FIGURES AND TABLES

1: ABSTRACT

Over the past fifteen years, glycerol dialkyl glycerol tetraethers (GDGTs) have increasingly been used to reconstruct ancient temperatures; paleoenvironmental proxies like TEX_{86} that correlate the relative abundance of these assumed archaeal cell membrane lipids to sea surface temperature are abundant in recent paleoclimatology literature. While it has become common to make reconstructions of past temperatures using GDGTs, our present understanding of the organisms that synthesize the compounds is still quite limited. The generally accepted theory states that microorganisms like *Thaumarchaeota* modify the structure of membrane lipids to increase intermolecular interactions, strengthening the membrane at higher temperatures. Yet to date, culture experiments have been largely restricted to a single species, *Nitrosopumilus maritimes*, and recent studies on oceanic archaeal rRNA have revealed that these biomarkers are produced in diverse, heterogeneous, and site-specific communities. This brings up questions as to whether different subclasses of GDGTs and all subsequent proxies represent adaptation within a single organismal group or a shift in community composition. Here, I examine distinct trends in compound-specific stable carbon isotope values ($\delta^{13}C$) of GDGTs extracted from the uppermost sediment in the Orca Basin, Gulf of Mexico, an intraslope basin on the Texas-Louisiana continental shelf featuring a brine lake in the bottommost 200m, using spooling-wire microcombustion isotope-ratio mass spectrometry (SWiM-IRMS). Lipid relative abundance data from the water column suggests a secondary zone of GDGT production above the seawater-brine transition with a greatly different ecology given GDGT-0 to crenarchaeol ratios and sediment $\delta^{13}C_{GDGT}$ values from a core thought record a retreat and expansion of the brine pool based on sedimentological and geochemical properties. The $\delta^{13}C$ values of all Orca Basin GDGTs are significantly heavier than those from open-marine Atlantic sites except for two the samples that correspond to the retracted brine which are statistically the same as the previously reported Atlantic values. Differential $\delta^{13}C$ traces between core depths that represent a sediment surface above vs. below the seawater/brine interface, particularly the shift in $\Delta^{13}C_{GDGT\text{-}0/Cren}$ from –0.64 to +0.21‰ and $\delta^{13}C_{GDGT\text{-}0}$ in general, show promise in helping to explain TEX_{86} non-linearity in high salinity, low-nutrient environments and the potential to serve as the backbone for new tetraether-based proxies for evaluating exogenous i.e. non-planktonic sourcing and measuring paleo-$\delta^{13}C_{DIC}$.

2: INTRODUCTION

At first glance, paleoclimatology seems more an art than a science. To capture something that is but fleeting in the scope of our human experience—the quiet after a thunderstorm, the scarlet night sky scrying snow, the sweltering summer heat of mirrored blue and brown—seems nigh impossible to record and recover. And yet the endeavor to reconstruct climate is a pursuit most integral to predicting and preparing for the future in face of a heavily human-modified carbon cycle. The development of new techniques and proxies that allow for quantitative assessments of past conditions has taken a principal role in the field of paleoclimatology, both as a means of evaluating broad scale changes in climatic variables like temperature or greenhouse gas concentrations through Earth's history, but also to better understand the relationships between records to tease out fundamental phenomena like our planet's temperature sensitivity to added atmospheric and marine CO_2 that can drastically alter modeled forecasts for the years to come (Lunt et al 2009).

Historically, paleoclimate — and in particular paleotemperature — reconstructions have been based on the geographic distribution or chemical composition of preserved body fossils, ranging from estimating terrestrial temperature gradients from assemblage-scale analysis of foliar physiognomy (Wolfe, 1993) and geographic distribution of fossil plant species (Greenwood and Wing, 1995), to the stalwart of marine temperature and continental ice volume calculated from oxygen isotopic composition of the calcareous tests of foraminifera (Erez and Luz 1983). The basic logic behind all of these proxy systems states that environmental conditions such as temperature, pH, salinity, alkalinity, atmospheric concentration of CO_2, etc., drive changes in biological characteristic like physiology, enzyme functionality, or species range and abiotic factors like rates of precipitation and incorporation into a crystal lattice, imprinting a signal of ancient climate that can be recovered and rediscovered in the present. Over the past 25 years, organic geochemists have expanded this conceptual framework to develop new techniques based on the distribution of 'biomarkers', or molecular fossils, including our man of the hour, GDGTs (Tierney 2014).

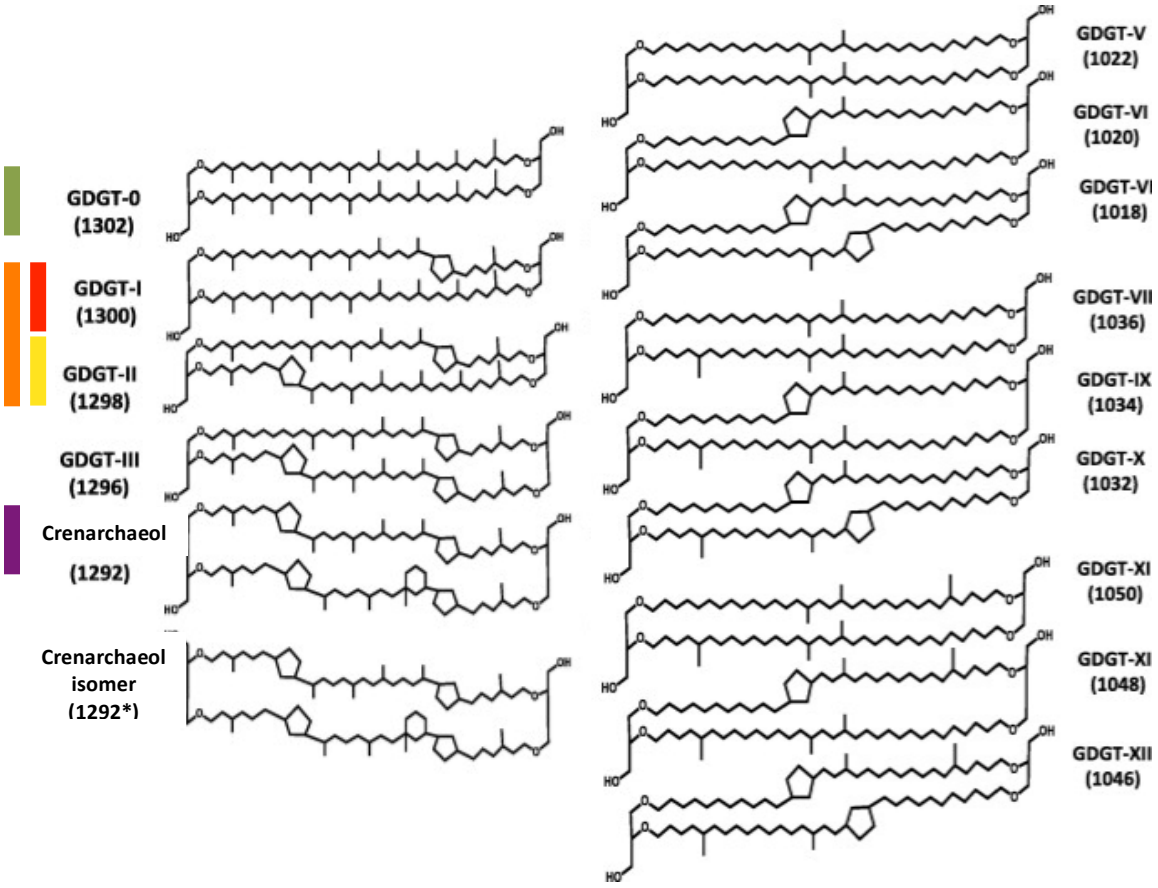

Figure 1: Schematic of GDGT chemical structure, listing name and mass to charge ratio. Bars next to GDGT-1, GDGT-1, GDGT-2, and Crenarchaeol mark the color these compounds will be represented by throughout this thesis. Adapted from Dirghangi et al 2013.

Glycerol dialkyl (or dibiphytanyl, there's a surprising degree of disagreement in the community) glycerol tetraether lipids (GDGTs) have in recent years become something of a golden boy to the paleoclimatology community (Figure 1). GDGTs are ubiquitous, both in space and time, and have been used in paleoclimate reconstructions spanning marine, lacustrine, and terrestrial settings from the Jurassic to the present (e.g. Tierney et al., 2010; Jenkyns et al., 2012, Peterse et al., 2012). They may be best known for comprising the TEX_{86} sea surface temperature (SST) proxy, but GDGT systems have also been proposed as a way to detect destabilization and dissociation of marine gas hydrates ("Methane Index", Zhang et al., 2010), whether TEX_{86} SST estimates deviate from modern analogues or are influenced by non-thermal factors ("Ring Index", Zhang et al., 2016), and even potentially track carbon isotopic composition changes in marine DIC (Hoefs et al., 1997; Schouten et al., 1998). Lipid biomarker based paleoclimate proxies such as TEX_{86} and

$U^{k'}_{37}$, a paleothermometry proxy based on alkenone lipids produced by haptophyte algae (Ho et al., 2013), rely on the assumption that unicellular organisms modify the composition of their cell membrane in order to maintain fluidity at different environmental temperatures (Tierney, 2014). This allows for the construction of paleotemperature records and other climatic variables independent of foraminiferal calcite, extending the range of paleoclimate and paleooceanography data sets to include sites where foram-based analyses be inaccurate given diagenetic processes or impossible in parts the ocean's basins that lie below the carbonate compensation depth (e.g. much of the Pacific).

There's a bit of a doublethink, or at least a compounding compositional factor, when considering that indices like the Methane Index and Ring Index operate under the assumption that GDGTs are produced by and preserved from diverse groups of organisms with preferences in tetraether production that are unrelated to temperature, i.e. the managing membrane fluidity hypothesis. Most studies to date cite that the GDGTs exported to the sediments are believed to be primarily produced by planktonic, ammonia-oxidizing *Thaumarchaeota* (Ouverney and Fuhrman, 2000), and these then swap GDGT moieties given temperature (Tierney, 2014; Schouten et al., 2013; and references therein). If that seems like a lot of qualifiers, it's because the jury is still out in regards to acknowledging other tetraether sources such as the *Euryarchaeota* (Lincoln et al., 2014), and as biogeochemists are better able to culture archaea in lab more and more variables appear to undermine or at lease question generalized assumptions regarding the mechanisms that control GDGT synthesis (Elling et al., 2014, 2015; Qin et al., 2015). Environmental studies have demonstrated that maximum cell numbers, copies of archaeal ammonia monooxygenase (*amoA*) and 16S rRNA genes occur at or just below the base of the photic zone (Church et al., 2010; Santoro et al., 2010); lipid abundances follow similar patterns (Lincoln et al., 2014; Xie et al., 2014), suggesting that the majority of planktonic thaumarchaeal activity and ergo GDGT synthesis is between 100 and 350m. However, sub-photic zone GDGT production cannot easily be distinguished from benthic or erosional sources.

Understanding the biological and post depositional factors impacting the recorded geological record is of utmost importance. Mankind's ability to accurately model predicted climate in a CO_2

enriched world were severely hampered through the 1990s and early 2000s by fundamental misunderstandings in the processes that occur within foraminifera from biological source to eventual geologic sink, especially through interpretations of diagenetically altered forams leading to the cool tropic paradox that stumped modelers for years (D'Hondt and Arthur 1996), an egregious error given that the much of the limited resource know as time was spent trying to recreate an artifact. The assumptions of planktonic, autotrophic, *Thaumarchaeota* dominance of GDGT production have not been rigorously tested. In regards to archaeal lipid carbon isotopic composition studies, variation outside of $\delta^{13}C$ values observed for suspended particulate matter—such as the -25‰ biphytane and GDGT values measured by Smittenberg et al. in 2006 and Biddle et al. in 2006—are simply deigned as anomalies caused by ^{13}C-depletion in the local DIC pool or in-situ heterotrophy by Archaea growing within the sediments (Pearson et al., 2016).

My thesis investigates $\delta^{13}C$ values of GDGTs recovered from sediments cored from the Orca Basin, and what ecological interpretations we can make by comparing the content of underlying sediments to GDGTs present in the water column above. Orca Basin serves as a particular example in the case of an oligotrophic water column overlying a stable pool of anoxic, hypersaline brine enriched in DOC (Shah et al 2013), which could signify a distinct nutrient cycle and remineralization regime from the open ocean. Those GDGT life histories, from carbon source to biosynthesis to eventual burial, will be recorded in $\delta^{13}C$ and serves as a useful comparison to the trends in $\delta^{13}C_{GDGT}$ of open marine Atlantic sites published earlier this year, the first study of its kind using spooling-wire microcombustion isotope-ratio mass spectrometer (SWiM-IRMS) to obtain carbon isotopic values for individual GDGTs (Pearson et al., 2016). Expanding the carbon isotope record of GDGTs is an important step in better understanding the organisms that are thought to be a major players in the global C and N cycling, the process of exporting GDGTs to the sediment, and how the interplay of these two factors can shape the relationships that underlie paleoclimate proxies. In other words, I am presenting results and initial data analysis and interpretation relating to the variance in Orca Basin compound-specific GDGT $\delta^{13}C$, and the implications that might have in regards to GDGTs' source, sink, and paleoclimate interpretations.

3: Study Area

Our story starts in the late Triassic, when roughly 200 million years ago Pangaea decided it was time to move on, to break up with itself, form the Gulf of Mexico. In a stint of Middle Jurassic (175–145 Ma) separation anxiety, the Gulf of Mexico was cut off from the ocean; as the tears/waters of this unnecessarily anthropomorphized body evaporated, it left behind a thick salt sheet, the Louann salt formation, which was later buried by new sediments (Pilcher and Blumstein, 2007; Cordes et al., 2009). Through the years, differential weight of sediments along the continental margin have caused deformation and movement of the salt layer, resulting in the Gulf's pockmarks of salt domes and brines that have been studied for over a hundred years (Washburne 1915).

The Orca Basin was the first deep-sea anoxic brine to be discovered in the Gulf of Mexico (Shokes et al., 1977). It is a 2,400-meter deep intraslope basin located in the northernmost region of the Gulf of Mexico, 200km southwest of the modern Mississippi Delta (Figure 2). It features an

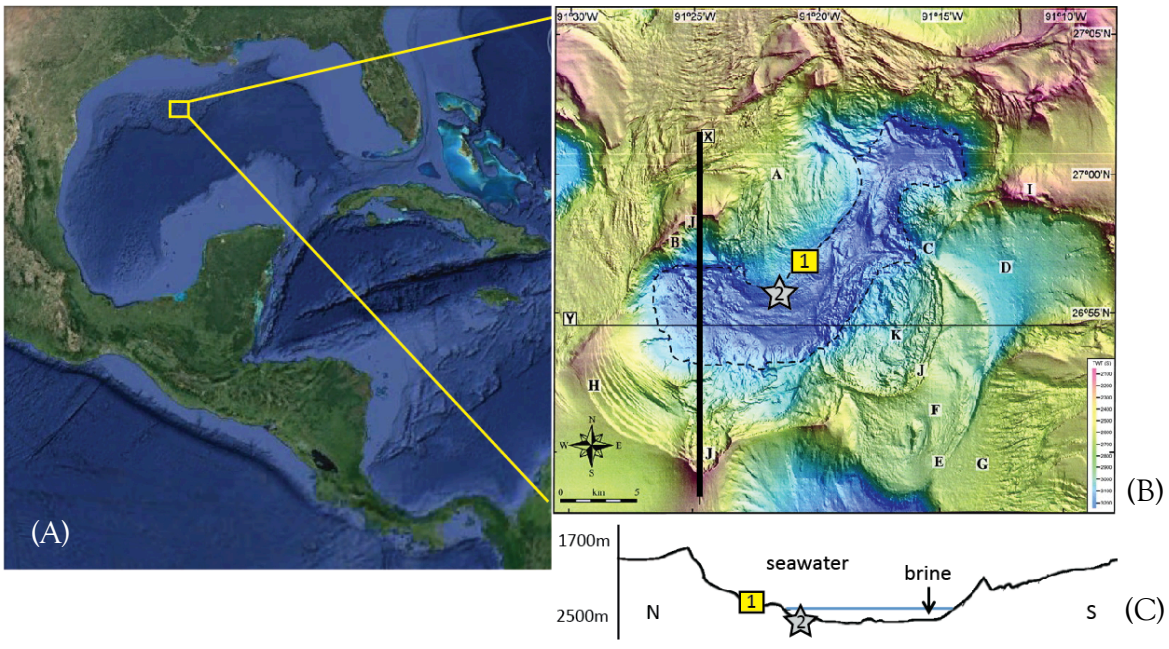

Figure 2: Core locations in Orca Basin, Gulf of Mexico, with location of Orca Basin in the greater Gulf of Mexico (A), seabed structure map of the Orca Basin and brine lake (B), and transect along the black line (C) with core OBI yellow box *1* and core OB grey star *2*. Adapted from Pilcher and Blumstein 2007.

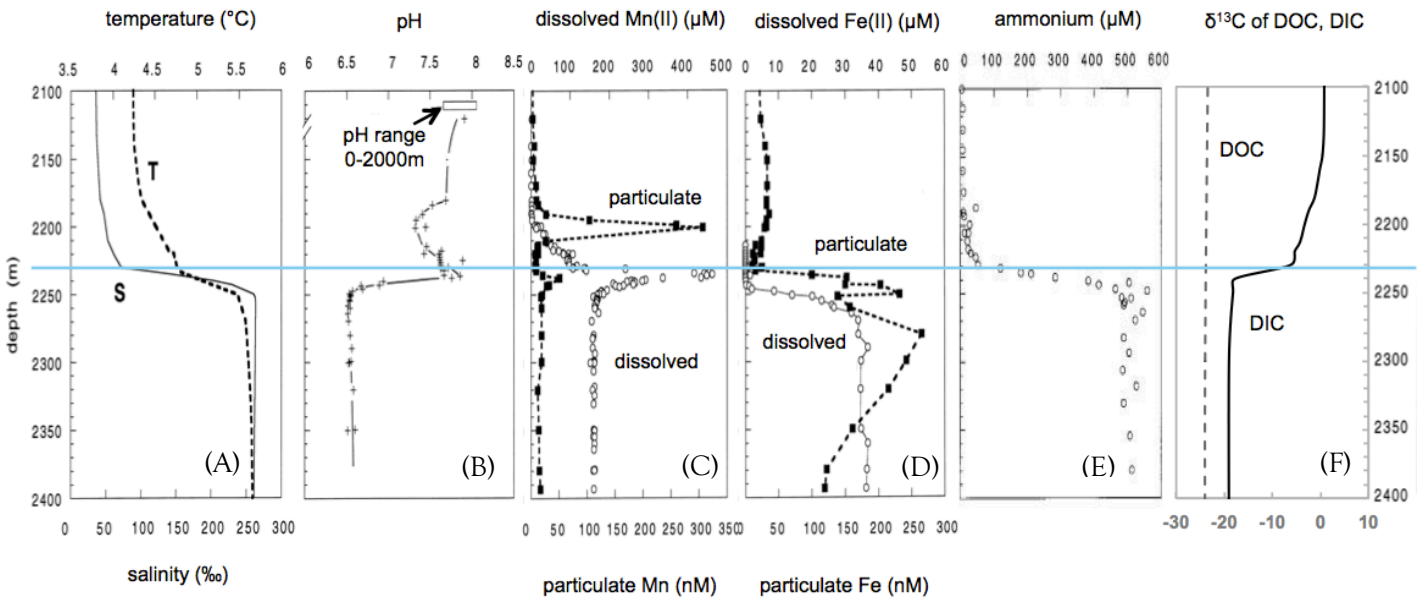

Figure 3: Geochemical composition of the Orca Basin brine pool. Panel (A) details the sharp salinity gradient starting at 2230m and the shallower temperature increase into the brine. The drop in pH (B) is thought to be the result of extensive manganese oxidation, evidenced by the shift in abundance of particulate and dissolved reduced manganese at and above the seawater-brine interface (C). Reduced iron becomes abundant in both dissolved and particulate form within the brine (D). Ammonium concentrations trace salinity (E). The carbon isotopic composition of DOC in the brine remains similar to water column values, though DIC becomes significantly deplete in ^{13}C within the brine pool, thought to be a combination of organic matter demineralization and methanogenesis (E). Adapted from van Cappellan et al., 1998 and Shah et al., 2013.

---

anoxic, hypersaline brine the bottom 180m of the water column, with a sharp salinity gradient from 70 to 260‰ between 2230 and 2250 meters depth (Figure 3a) (van Cappellen et al., 1998). Radiocarbon ages suggest that the brine was established 8,700 ± 100 years ago (Shah et al., 2013); the geochemistry of the brine and the composition of underlying sediments indicate that the brine is formed by dissolution of nearby salt exposures and lateral advection of the brine to the basin (Pilcher and Blumstein, 2007; Shokes et al., 1977), unlike many other Gulf of Mexico brines that have in situ sources (Joye et al., 2005; Shah et al., 2013). Surface water conditions and seasonal productivity are considered normal within the broader context of the Texas-Louisiana continental shelf, but the brine pool is noted both for its unusual formation mechanism and biogeochemical properties and microbial activity (Antunes et al., 2011; van Cappellen et al., 1998)

Oxygen and nitrate are not detectable within the brine, while phosphate concentrations are elevated relative to overlying seawater due to the decomposition of organic-matter (Shokes et al.,

1977; van Cappellen et al., 1998). The accumulation of demineralized organic matter is quite apparent from the dramatic decline in the $\delta^{13}C$ value of DIC through the transition zone into the brine (Figure 3f), though the biological production of methane has also been suggested as contributing factor (Zhuang 2014). While sulfate concentrations are not depleted within the brine (Trefry et al., 1984; Hurtgen et al., 1999), suggesting limited microbial sulfate reduction, there is strong evidence for intense microbial activity at the seawater-brine interface, observed to act as a particle trap with successive depletion of oxygen, nitrate, and oxidized manganese (Trefry et al., 1984; van Cappellen et al., 1998), with an accumulation of dissolved and particulate reduced iron coinciding with a drop in pH to 6.5 the first 20 to 50m of the brine pool (Figure 3a-f) leading to van Cappellen's conclusion that acid-base chemistry, redox transformations, and microbial metabolic activity within the transition zone are largely controlled by intense microbial redox cycling of manganese, ultimately controlled by the slow rate of Mn loss from the sediments through the brine. In untangling the history of the GDGTs recovered at this location, it become extremely important to understand the potential for various forms of chemoautotrophy at depths that could contribute to the exported GDGT pool, especially considering that radiocarbon values radiocarbon values point to the seawater-brine interface region as the likely source for much if not most brine DOC and DIC (Shah et al 2013).

4: METHODS

4.1 Samples

GDGTs were isolated from 9 total lipid extracts (TLEs) derived from two sediment cores collected from the Orca Basin in the Gulf of Mexico (Table 1). All samples were collected between April 10 and April 14, 2012, during a research cruise on the RV *Pelican* operated by the Louisiana Universities Marine Consortium (LUMCOM). The cores were sub-sectioned into half centimeter depth-wise samples by Courtney Warren and have been stored at -20°C since collection. Seven horizons were sampled from the intermediate-central-basin core OB-0412-MC-0502C (OBI), two from core OB-0412-0502A (OB). The location of these two cores in relation to the extent of the

Table 1:
Sediment sample compound concentration, relative abundance, and $\delta^{13}C_{GDGT}$

Sample Name	OB 0.5cm	OB 4.0cm	OBI 8.5cm	OB 15.5cm	OB 22.0cm	OB 26.0cm	OB 46.0cm	OB 50.0cm	OB 64.0cm
Sample Information									
Core	OB	OB	OBI	OBI	OBI	OBI	OBI	OBI	OBI
Horizon	0.5-1.0cm	4.0-4.5cm	8.5-9cm	15.5-16.0cm	22.0-22.5	26.0-26.5cm	46.0-46.5cm	50.0-50.5cm	64.0-64.5cm
Compound Abundances: mg GDGT/g sediment									
GDGT-0	2.36	1.45	1.16	1.56	1.48	1.44	0.41	0.45	1.60
GDGT-1				1.04					1.05
GDGT-1+2	3.12	1.41	1.08	2.04	1.63	1.84	0.42	0.54	2.13
GDGT-2				1.00					1.07
Crenarchaeol	5.06	4.47	3.39	3.77	3.70	2.99	1.03	1.21	4.35
GDGT Relative Abundance: fraction of total GDGT mass									
GDGT-0	0.22	0.20	0.21	0.21	0.22	0.23	0.22	0.21	0.20
GDGT-1				0.14					0.13
GDGT-1+2	0.30	0.19	0.19	0.28	0.24	0.29	0.23	0.25	0.26
GDGT-2				0.14					0.13
Crenarchaeol	0.48	0.61	0.60	0.51	0.54	0.48	0.55	0.55	0.54
GDGT/Crenarchaeol Ratios									
GDGT-0	0.47	0.33	0.34	0.41	0.40	0.48	0.40	0.37	0.37
GDGT-1+2	0.62	0.31	0.32	0.54*	0.44	0.62	0.41	0.45	0.49*
GDGT/GDGT-0 Ratios									
GDGT-1+2	1.32	0.97	0.94	1.31	1.09	1.27	1.04	1.19	1.32
Crenarchaeol	2.15	3.08	2.92	2.41	2.49	2.07	2.53	2.67	2.71
$\delta^{13}C$ (‰)									
GDGT-0	−18.4 ± 0.1	−18.2 ± 0.2	−18.2 ± 0.2	−18.2 ± 0.1	−18.1 ± 0.0	−18.3 ± 0.1	−19.4 ± 0.3	−19.2 ± 0.1	−18.1 ± 0.1
GDGT-1				−18.4 ± 0.1					−18.5 ± 0.2
GDGT-1+2	−18.9 ± 0.1	−18.6 ± 0.1	−18.5 ± 0.0	−18.6 ± 0.1*	−18.5 ± 0.1	−18.7 ± 0.1	−19.5 ± 0.1	−19.5 ± 0.3	−18.6 ± 0.2*
GDGT-2				−18.8 ± 0.2					−18.8 ± 0.2
Crenarchaeol	−18.7 ± 0.1	−18.3 ± 0.1	−18.7 ± 0.1°	−18.3 ± 0.3	−18.1 ± 0.2	−18.4 ± 0.2	−18.6 ± 0.3	−18.7 ± 0.2	−18.4 ± 0.1

* combined from independent measurements of GDGT-1 and GDGT-2

° this $\delta^{13}C$ value is considered suspect. The peak appeared overloaded, suggesting a value closer to -18.2‰

modern brine pool are detailed in Figure 2b and 2c, with core OBI represented by the location of the yellow square labeled "1", and core OB by the grey star labeled "2". Half-centimeter sections of the core were freeze-dried, extracted, and run through silica-gel chromatography at Yale and submitted to the Pearson Lab at Harvard for SWiM-IRMS analysis. Results are shown as a collapsed data set of samples from both cores; the interior-basin core OBI was sampled a horizons of depths 0.5-1.0cm and 4.0-4.5cm, and as such appear as the two uppermost samples in subsequent figures.

GDGT relative abundance data for the Orca Basin water column was provided by Felix Elling. Water column samples were collected on the same research expedition as the sediment cores, using pumps provided by Woods Hole Oceanographic Institute, the University of Florida, and the Georgia Institute of Technology. Between 4 and 3088 liters of seawater were pumped through the filter at each given depth. All pumps were fitted with a 0.2µm-mesh Durapore filter, for which the collected organic matter is presumed to be better representative of in-situ production (Table 2), and a 5µm-mesh Nitex pre-filter designed to filter out lipids aggregated with other organic matter and record a particulate organic matter-type signal (Table 3). Pumps were fitted with a second. The primary data collected from this cruise is currently unpublished, and presented here with the permission of Felix Elling and Courtney Warren. Sample collection at some depths is known to have been impacted by pump mechanical failures, and suspect depths or those with missing data are identified either by a superscript symbol († for 0.2µm filter data, § for 5µm pre-filter data) or marked in figures as an 'x' and removed from trend lines. No GDGT concentration estimates I received have been excluded from this thesis, but qualifications for water-depth measurement inclusion in further steps of this project may need to be refined and reexamined.

4.2 Extraction and processing

After retrieval from –20°C storage, sediment samples were freeze-dried to remove water, leaving behind noticeable salt crystals on the exterior surface of what used to be mud. TLEs were extracted via accelerated solvent extraction (ASE) in 2:1 DCM: MeOH. TLEs were separated over SiO_2 (130–270 mesh) into five fractions: three fractions of less-polar compounds (100% hexane, 10%v

Table 2:
Water column compound abundance on 0.2μm filters

Depth	*GDGT Concentration (ng/L)*					*GDGT/Crenarchaeol ratios*			*GDGT/GDGT-O ratios*		
(m)	GDGT-0	GDGT-1	GDGT-2	GDGT-1+2	Cren	GDGT-0	GDGT-1	GDGT-2	GDGT-	GDGT-2	Cren
5	0.25	0.10	0.13	0.23	0.52	0.48	0.19	0.26	0.40	0.53	2.07
60	1.12	0.39	0.58	0.97	2.85	0.39	0.14	0.20	0.35	0.52	2.54
80	5.69	2.01	1.95	3.96	13.36	0.43	0.15	0.15	0.35	0.34	2.35
120	3.75	1.47	3.22	4.68	13.24	0.28	0.11	0.24	0.39	0.86	3.53
200	0.80	0.27	0.52	0.79	1.62	0.49	0.17	0.32	0.34	0.65	2.02
250	2.75	0.74	1.34	2.07	5.43	0.51	0.14	0.25	0.27	0.49	1.97
300	3.85	1.42	2.64	4.06	9.86	0.39	0.14	0.27	0.37	0.69	2.56
400†	0.00	0.00	0.00	0.01	1.89	0.00	0.00	0.00	1.41	1.11	793.88
500†	4.14	0.00	0.00	0.00	8.00	0.52	0.00	0.00	0.00	0.00	1.93
600	9.34	3.29	4.93	8.21	21.75	0.43	0.15	0.23	0.35	0.53	2.33
800	2.79	0.97	1.22	2.19	4.01	0.69	0.24	0.30	0.35	0.44	1.44
1000	0.65	0.20	0.20	0.41	0.93	0.70	0.22	0.22	0.31	0.31	1.43
1250	4.21	1.32	1.70	3.02	7.57	0.56	0.17	0.22	0.31	0.40	1.80
1500†	0.00	0.00	0.00	0.00	0.00						
1900	3.84	1.36	1.70	3.06	7.30	0.53	0.19	0.23	0.35	0.44	1.90
2000	2.57	0.80	1.05	1.85	4.56	0.56	0.18	0.23	0.31	0.41	1.77
2100	0.77	0.25	0.29	0.54	1.40	0.55	0.18	0.21	0.32	0.38	1.81
2150	14.64	4.23	3.48	7.71	18.36	0.80	0.23	0.19	0.29	0.24	1.25
2176	31.15	8.51	5.95	14.46	30.54	1.02	0.28	0.19	0.27	0.19	0.98
2190	19.75	3.52	2.28	5.80	17.87	1.11	0.20	0.13	0.18	0.12	0.90
2200	6.47	1.22	0.77	1.99	5.12	1.26	0.24	0.15	0.19	0.12	0.79
2212	6.92	1.40	1.04	2.44	5.39	1.29	0.26	0.19	0.20	0.15	0.78
2220	28.66	3.37	1.83	5.20	14.54	1.97	0.23	0.13	0.12	0.06	0.51
2235	8.96	1.25	0.89	2.14	5.32	1.68	0.24	0.17	0.14	0.10	0.59
2242	19.54	2.70	1.74	4.45	13.63	1.43	0.20	0.13	0.14	0.09	0.70
2250	9.58	1.60	1.62	3.21	7.15	1.34	0.22	0.23	0.17	0.17	0.75
2270	2.58	0.40	0.35	0.74	1.77	1.46	0.22	0.20	0.15	0.14	0.69
2290†	10.16	0.00	0.00	0.00	0.00				0.00	0.00	0.00
2300	1.85	0.43	0.37	0.80	1.50	1.23	0.28	0.25	0.23	0.20	0.81

† depths where GDGT concentrations were measured as 0.00ng/L. As a significant deviation from the rest of the water column, measurements for these depths are likely inaccurate either by way of analytical or collection error and are marked as 'x's in figures of water column characteristics.

Table 3:
Water column compound abundance on 5μm filters

Depth	*GDGT Concentration (ng/L)*					*GDGT/Crenarchaeol ratios*			*GDGT/GDGT-O ratios*		
(m)	GDGT-0	GDGT-1	GDGT-2	GDGT-1+2	Cren	GDGT-0	GDGT-1	GDGT-2	GDGT-1	GDGT-2	Cren
5	0.43	0.04	0.03	0.08	0.32	1.32	0.14	0.10	0.10	0.07	0.76
60	0.17	0.05	0.08	0.13	0.39	0.43	0.14	0.20	0.32	0.47	2.34
80	2.87	1.09	1.25	2.34	8.73	0.33	0.12	0.14	0.38	0.44	3.04
120	0.40	0.09	0.12	0.21	0.54	0.74	0.17	0.23	0.23	0.31	1.35
200	0.27	0.09	0.16	0.25	0.37	0.72	0.23	0.43	0.32	0.59	1.38
250	4.88	0.90	1.41	2.31	8.51	0.57	0.11	0.17	0.18	0.29	1.75
300§	0.59	0.00	0.00	0.01	1.43	0.41	0.00	0.00	0.00	0.00	2.43
400§	0.00	0.01	0.00	0.01	2.69	0.00	0.00	0.00	2.65	1.58	916.54
500§	0.00	0.00	0.00	0.00	3.89	0.00	0.00	0.00			
600§	0.00	0.00	0.00	0.00	0.00						
800	1.32	0.43	0.67	1.10	2.21	0.60	0.19	0.30	0.32	0.51	1.68
1000	1.60	0.56	0.73	1.29	2.80	0.57	0.20	0.26	0.35	0.45	1.75
1250	1.12	0.38	0.49	0.87	2.20	0.51	0.17	0.22	0.34	0.44	1.96
1500	3.33	1.15	1.59	2.74	6.05	0.55	0.19	0.26	0.35	0.48	1.82
1900	0.70	0.22	0.29	0.51	1.17	0.60	0.19	0.25	0.32	0.41	1.68
2000	0.23	0.08	0.08	0.16	0.38	0.59	0.20	0.21	0.34	0.36	1.68
2100	0.32	0.09	0.12	0.22	0.54	0.60	0.17	0.23	0.28	0.39	1.66
2150	0.83	0.22	0.23	0.45	0.98	0.85	0.23	0.23	0.27	0.28	1.18
2175	3.05	0.80	0.70	1.50	3.52	0.87	0.23	0.20	0.26	0.23	1.15
2190	1.22	0.22	0.19	0.41	1.10	1.11	0.20	0.17	0.18	0.16	0.90
2200	2.70	0.65	0.48	1.13	2.73	0.99	0.24	0.17	0.24	0.18	1.01
2212	18.37	3.59	2.77	6.37	15.86	1.16	0.23	0.17	0.20	0.15	0.86
2220	6.17	1.19	0.94	2.13	5.94	1.04	0.20	0.16	0.19	0.15	0.96
2235	5.96	1.29	1.35	2.63	6.89	0.87	0.19	0.20	0.22	0.23	1.16
2242	12.06	3.17	3.48	6.65	18.63	0.65	0.17	0.19	0.26	0.29	1.54
2250	2.15	0.58	0.53	1.11	2.26	0.95	0.25	0.24	0.27	0.25	1.05
2270	1.32	0.29	0.34	0.63	1.48	0.90	0.20	0.23	0.22	0.26	1.12
2290	50.90	20.44	15.44	35.88	61.87	0.82	0.33	0.25	0.40	0.30	1.22
2300	1.54	0.50	0.51	1.01	2.13	0.72	0.23	0.24	0.33	0.33	1.38

§ depths where GDGT concentrations were measured as 0.00ng/L. As a significant deviation from the rest of the water column, measurements for these depths are likely inaccurate either by way of analytical or collection error and are marked as 'x's in figures of water column characteristics.

ethyl acetate:hexane, 25%v ethyl acetate:hexane), GDGT core lipids (1:1v ethyl acetate:hexane), and polar compounds (100% ethyl acetate, followed by 100% methanol) in same protocol as previous $\delta^{13}C_{GDGT}$ study (Pearson et al., 2016).

4.3 HPLC methods

The isolation and identification of individual GDGT moieties was conducted under the column and solvent gradient protocol as previously established (Ingalls et al., 2006, Shah and Pearson 2007, Shah et al., 2008). The total GDGT fraction for each sample is first separated by normal phase (NP) high-performance liquid chromatography (HPLC) such that each individual GDGP moiety is independently recollected. Time windows for compound-specific NP-HPLC collection windows are standard as per protocol screening a preliminary sample by atmospheric pressure chemical ionization-mass spectrometry (APCI-MS). Following NP-HPLC, GDGT concentrations are estimated by semi-quantitative flow injection analysis (FIA), estimating concentrations of sample relative to a dilution series of synthetic standard C_{46}-GDGT (Huguet et al., 2006). This is done both to limit the amount of material injected for subsequent reverse phase (RP) HPLC to *ca.* 20µg total GDGT, minimizing the risk of column overload and improving chromatographic separation (Ingalls et al 2006, Shah and Pearson, 2007; Shat et al., 2008), as well as to asses which samples contained large enough quantities of GDGT-1 and GDGT-2 to obtain individual $\delta^{13}C$ measurements or if the GDGT-1 and GDGT-2 NP-HPLC fractions would need to be combined for a joint GDGT-1+2 value.

NP-HPLC is followed further purification via RP-HPLC to remove non-tetraether material. All targeted GDGTs (GDGT-0 through crenarchaeol) elute in a window of roughly one minute by RP-HPLC; the preceding minute, the GDGT fraction, and the tailing minute are collected as three separate fractions. The purified GDGT fractions are dried under N_2 and dissolved in 25µl ethyl-acetate for IRMS; RP-HPLC, IRMS, and a final post-IRMS FIA analysis of the remaining material are always performed on the same day.

4.4 SWiM-IRMS

Post RP-HPLC, values of $\delta^{13}C_{GDGT}$ are measured via Spooling Wire Microcombustion-IRMS, or SWiM-IRMS, a technique that was first presented as a method for obtaining high-precision $\delta^{13}C$ values for relatively small samples sizes by Brand and Dobberstein in 1916 (apparently the editor insisted on a catchy acronym). SWiM-IRMS allows for $\delta^{13}C$ measurement precision better than 0.2‰ for samples containing as little as 25ng of carbon (Sessions et al., 2005), which proved essential to this study given the low abundance of GDGTs within a 0.5cm segment of a core. SWiM-IRMS remains a technique that requires the construction of an in-house system, which whimsically (and also pragmatically) uses a fishing rod reel as the collection spool noted in the schematic above (Figure 4), but it has now been used in the pursuit of a broad array of questions, ranging from analyzing the stable carbon isotopic composition of individual grains of pollen (Nelson et al., 2007), to measuring $\delta^{13}C$ on the order of 100 bacterial cells (Eek et al., 2007).

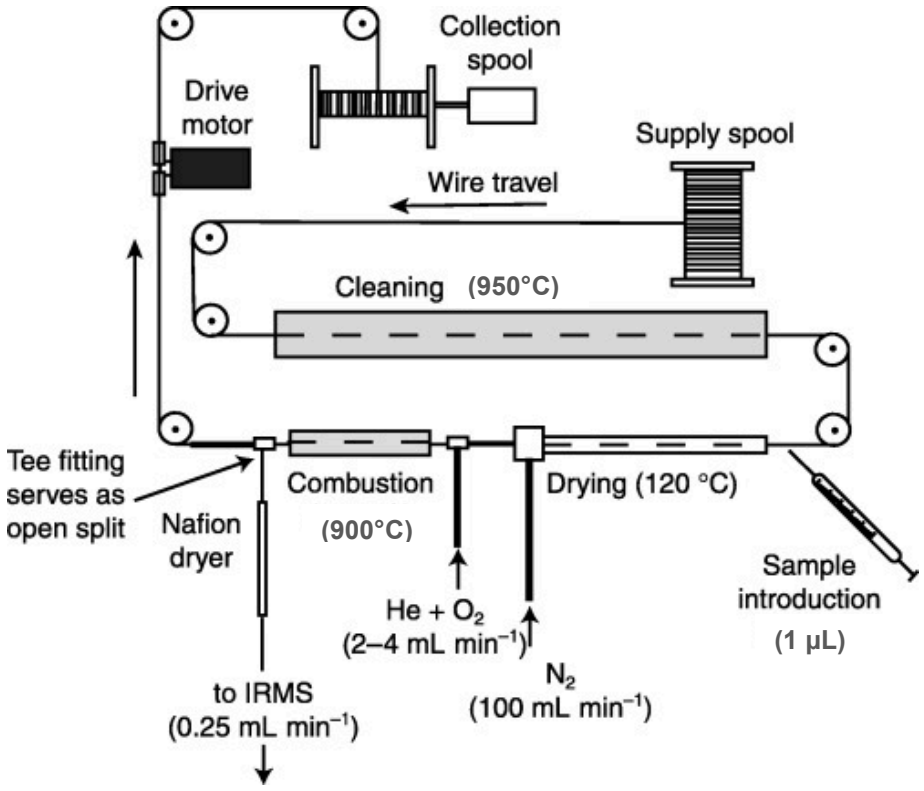

Figure 4: Schematic for Harvard Department of Earth and Planetary Sciences SWiM-IRMS set up. Modifications for GDGT analysis include cleaning oven temperature of 950°C and combustion at 900°C. Adapted from Eek et al., 2007.

The configuration and operation of a SWiM-IRMS system is described in detail in the above mentioned Brand and Dobberstein, Nelson et al., and Sessions et al. papers, but in short the process goes like this: 1µl of sample dissolved in ethyl acetate is deposited using a syringe onto a pre-oxidized nickel wire which then moves into a combustion, combusting the sample into CO_2 which is then separated from H_2O in a Naflong drying tube and transferred to the IRMS through an open split. My Orca Basin samples were analyzed using the SWiM-IRMS system set up at the Harvard Department of Earth and Planetary Sciences, which operates similarly to that of Sessions et al. (2005) with a few modifications for measurement of GDGTs. Namely the cleaning furnace runs at 950°C, the combustion furnace at 900°C, and there is a ceramic combustion reactor with modified gas flow (Mohr et al., 2014). Each sample SWiM-IRMS analysis is run in quintuplicate, at 30-second intervals. SWiM-IRMS quantifications of total CO_2 generated are don via comparison of sample results to a C_{46} GDGT standard dilution series.

5: RESULTS

The following presents initial analytical results and trends from Orca Basin sediments. Suggestions for additional measurements and statistical tests can be found at the end of the discussion section.

5.1: GDGT distribution in sediments

The relative abundance of GDGT-0, GDGT-1, GDGT-2, and crenarchaeol more closely align with the relative abundance of tetraether compounds in the upper water column as opposed to the GDGT-0 shifted distribution within the brine pool (Figure 5a-b), with on average 21 ± 1% GDGT-0, 25 ± 4% GDGT-1 and -2 combined, and 54 ± 5% crenarchaeol (Table 1). The relative GDGT-1+2 and crenarchaeol abundance are inversely related in the sediment, with GDGT-1+2 ranging from 19% to 30%, crenarchaeol 48% and 61%, where [GDGT-1+2]*[Cren] = 0.13 ± 0.01. In comparison, [GDGT-1+2]*[GDGT-0] = 0.05 ± 0.01. The depths with the lowest amount of crenarchaeol (and greatest GDGT-1+2) appear to be the dark black sediment horizons at 0.5cm, 15.5 and 26.0cm.

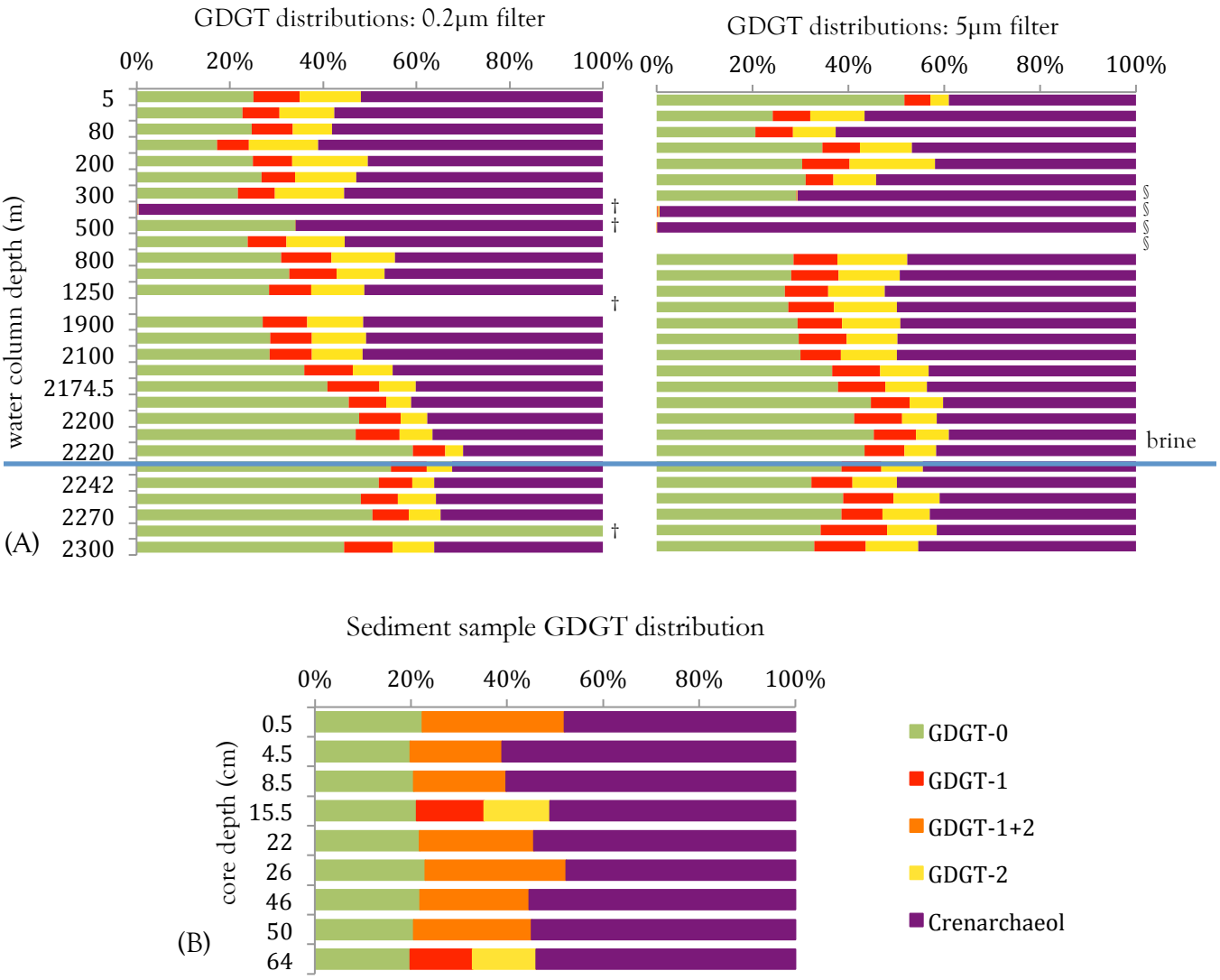

Figure 5: Distribution of GDGT-0, GDGT-1, GDGT-2, and Crenarchaeol in Orca Basin water column and sediment sample extracts. Relative abundance in ng/L for water column samples extracted from 0.2µm and 5µm filters (a). Water column depths with reported lack of one or more moieties are marked with † (0.2µm filters) or § (5µm filters) as in Table 2 and Table 3 and considered suspect. The equivalence of depth 2300m is marked with the brine pool line. Sediment sample distributions are in µg GDGT per g (b).

The concentration of µg GDGT per g sediment is lower by over a factor of 3 at depths 46cm and 50cm relative to the other sample, with an average of: 0.43 ± 0.03µg/g vs. 1.58 ± 0.4µg/g GDGT-0, 0.48 ± 0.08µg/g vs. 1.98 ± 0.65µg/g GDGT-1+2, and 1.12 ± 0.13µg/g vs. 4.00 ± 0.76µg/g for Crenarchaeol. Measured individually in samples at 15.5cm depth and 64.5, the concentration of GDGT-1 and GDGT-2 were 0.14 ± 0.0µg/g sample (Figure 6b; Table 1).

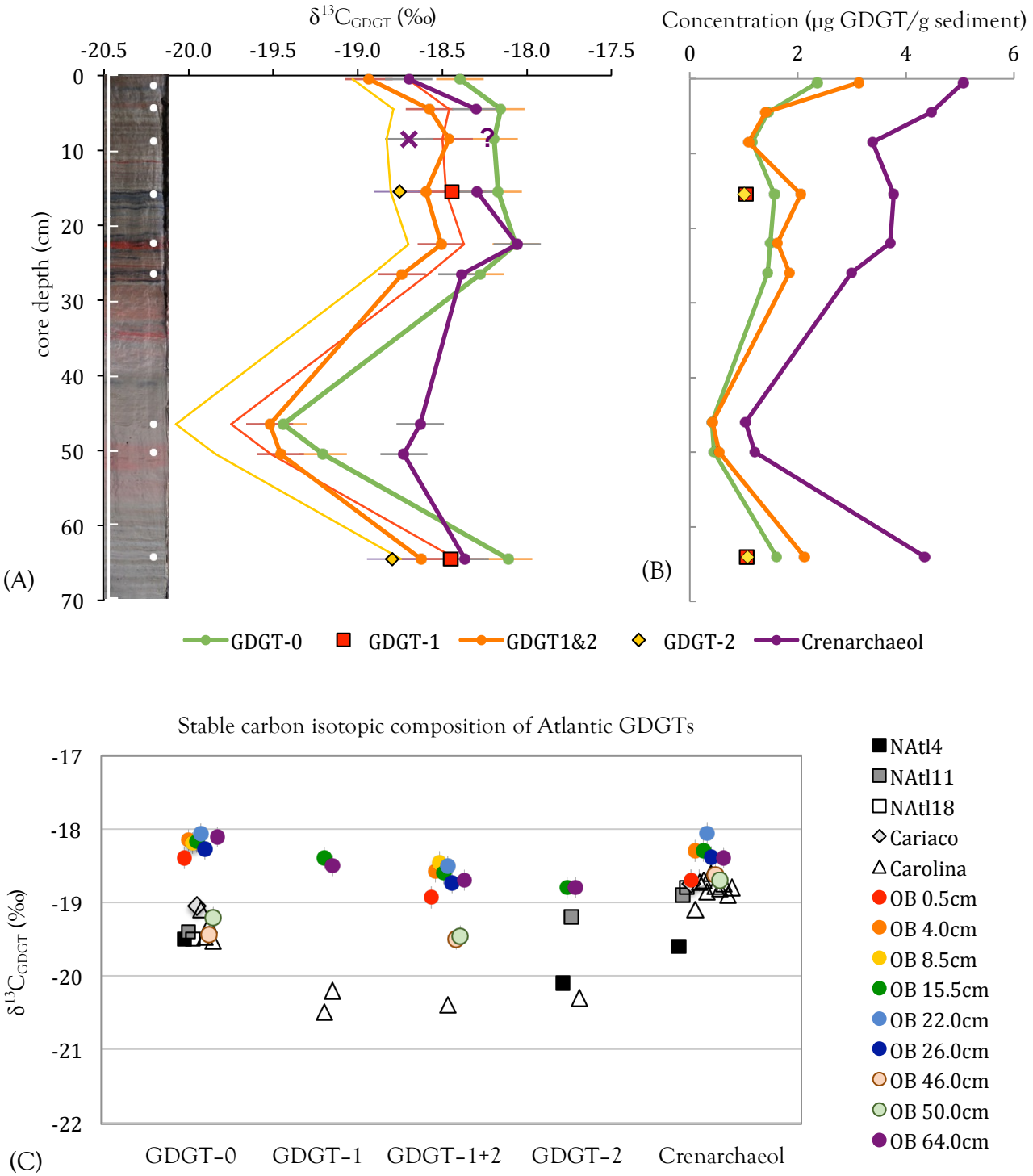

Figure 6: Isotopic and abundance results for Orca Basin sediment samples. Carbon isotopic values (A) and concentrations (B) of GDGTs isolated from Orca Basin sediments are plotted next to a to-scale image of core OB-0412-MC-0502C, with sampled bands marked with a white dot. GDGT-0 is green, GDGT-1 is red, combined GDGT1+2 orange, GDGT-2 yellow, and crenarchaeol purple. The thin yellow and red lines in (A) are projected values for GDGT-1 and -2 assuming isotopic offset between -0, -1, and -2 the same at all depths. Note that the $\delta^{13}C$ value for Crenarchaeol at 8.5cm (marked **x**) yielded an overloaded peak and as such is considered suspect, with a likely isotopic value of -18.2‰ (marked **?**), and has been excluded from plot (C), which details $\delta^{13}C_{GDGT}$ values from Orca Basin and Atlantic sites NAtl4, Natl11, Natl18, Cariaco, and Carolina published in Pearson et al. 2016.

5.2: Orca Basin $\delta^{13}C_{GDGT}$

The $\delta^{13}C_{GDGT}$ values for crenarchaeol the from all depths in the Orca Basin section are statistically the same, –18.46 ± 0.24‰, as is the isotopic offset between GDGT-0 and GDGT-1+2 ($\Delta^{13}C_{0/1+2}$) at –0.38 ± 0.15‰, given average SWiM-IRMS measurement precision determined to be ±0.25‰ from 10 repeated evaluations of Carolina margin crenarchaeol isolate $\delta^{13}C$ over the course of four months (Pearson et al. 2016). However, the isotopic composition of GDGT-0 and GDGT-1+2 and inter-GDGT isotopic offsets $\Delta^{13}C_{0/Cren}$ and $\Delta^{13}C_{1+2/Cren}$ behave in ways that suggest a 2-state system. Depths 0.5cm, 4.5cm, 8.5cm, 15.5cm, 22.0cm, 26.0cm, and 64.0cm are all statistically equivalent in $\delta^{13}C_{GDGT\text{-}0}$ (–18.19 ± 0.11‰), $\delta^{13}C_{GDGT\text{-}1+2}$ (–18.63 ± 0.16‰), $\Delta^{13}C_{0/Cren}$ (0.16 ± 0.11‰) and $\Delta^{13}C_{1+2/Cren}$ (–0.31±0.08‰) (Table 1). Calculations exclude the crenarchaeol measurement from 8.5cm depth: non-Gaussian distribution indicated an overloaded peak, which result in a measurement estimated to be 0.5‰ lighter than real value, which is marked with the (x) and (?) in Figure 6a. Depths 46.0cm and 50.0cm behave identically to one another, with isotopic values of $\delta^{13}C_{GDGT\text{-}0}$ (–19.32 ± 0.17‰) and $\delta^{13}C_{GDGT\text{-}1+2}$ (–19.49 ± 0.05‰) and offsets $\Delta^{13}C_{0/Cren}$ (–0.64 ± 0.24‰) and $\Delta^{13}C_{1+2/Cren}$ (–0.81±0.11‰). It should be noted that in both in both subsets of samples, the carbon isotopic offset between GDGT-1+2 and Crenarchaeol is more highly correlated than the offset between GDGT-0 and Crenarchaeol.

Binning $\delta^{13}C_{Cren}$ and $\Delta^{13}C_{0/1+2}$ into these two depth subsets results in a noticeable offset in average value and decrease in 1σ , with $\delta^{13}C_{Cren}$ equal to –18.68±0.7 for depths 46.0cm and 50.0cm, and –18.35±0.21‰ for the rest; $\Delta^{13}C_{0/1+2}$ then contracts to –0.17 ± 0.12‰ for 46.0cm and 50.0cm and expands to –0.44 ± 0.09‰ for the rest of the depth profile. These values present two different relationships between GDGT isotopic composition, both in absolute value and sign. The first corresponds with trends observed in other open-marine Atlantic sites, where Orca Basin 46.0cm and 50.0cm plus other Atlantic $\delta^{13}C_{GDGT\text{-}0}$ is –19.4‰ with a minor GDGT signal that is isotopically lighter and crenarchaeol values enriched in ^{13}C by 0.6‰ at a value of –18.8‰ for all values excluding NAtl4 (Pearson et al 2016, Figure 6c). The other Orca Basin sites yield markedly different trends, with $\delta^{13}C_{GDGT\text{-}0}$ at –18.2‰, still a lighter minor GDGT signal, but crenarchaeol values depleted in ^{13}C by 0.2‰ at –18.4‰, a similar $\Delta^{13}C_{0/Cren}$ to NAtl4 (Figure 6c, Table 4).

NAtl4 was previously presented as a potential undetected analytical, as NAtl4 $\Delta^{13}C_{0/Cren}$ broke the Pearson et al. 2016 observed trend of a C^{13} enriched Crenarchaeol signal in relation to GDGT-0. The $\Delta^{13}C_{0/Cren}$ relationship established in Orca Basin sediments, anomalously light by open-marine Atlantic standards, would bolster an alternative hypothesis that the altered relationship between GDGT-0 and Crenarchaeol reflect exogenous GDGT input potentially related to fluxes from the Gulf of St. Lawrence to NAtl4's location and changing brine pool dynamics in the Orca Basin.

5.3: Trends in sedimentology

Core OB-0412-MC-0502C (OBI) has distinct shifts in coloration, and likely chemical composition, which correspond to difference in $\delta^{13}C_{GDGT}$ (Figure 6a, Figure 7). The top 27cm are primarily composed of finely, sub-centimeter-scale laminated interbedded layers of light and dark grey with punctuated bands of bright red (22.0cm) and black (26.0cm). From 28cm to 56cm, the core loses the thin, well defined lamination instead consisting of a sequence bounded by a dull red, ~4cm thick band at the top, two wide dull red bands at the bottom, and grey mud with an occasional splash of black or bright red in between. From 57cm to the bottom of the core at 70cm, there is a return to interbedded light and dark grey, >1cm wide banding. These types of sediment coloring have been previously noted in Orca Basin cores (Hurtgen et al., 1999; Meckler et al., 2008), but not within the same core. Samples OB46.0cm and OB50.0cm, the two depths that fall within the middle package of lighter sediment with multi-centimeter red layers and lack microlaminations, produced results that do not correspond with the carbon isotopic values, carbon isotopic offsets, and GDGT concentrations of the samples located in the upper or lower parts of the core (Table 1).

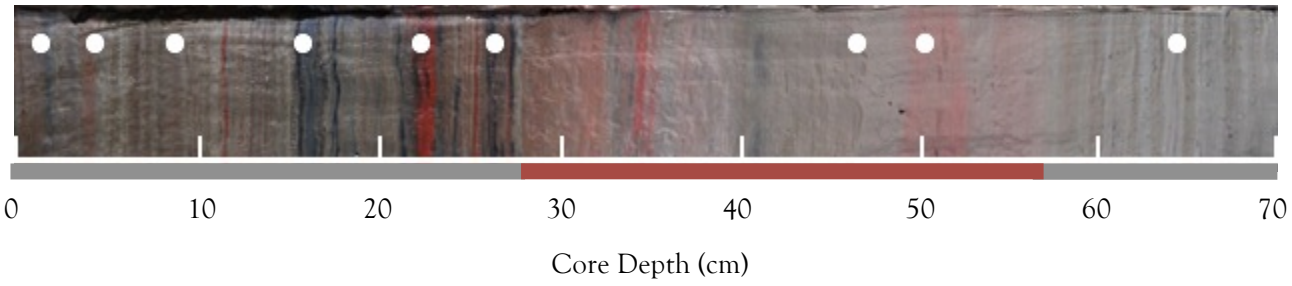

Figure 7: Close-up of core OB-0412-MC-0502C. Image has been modified to saturation 100% and brightness +20% to improve visibility of color contrasts. Bar at the bottom marks depth in 10cm increments, with white dots noting sample locations. Discreet sedimentation packages of 0-28cm, 28cm-57cm, and 57cm to 70cm, defined by changes in bed thickness and color, are marked by the grey and red bars along the bottom of the core.

6: DISCUSSION, AKA FOOD FOR FURTHER THOUGHT

6.1: Water column GDGTs and the feasibility of production at depth

If we use the concentration of GDGTs collected on the 0.2µm filters as signal of in-situ production, and trust the quantification scheme and extraction method for plastic filters used by Felix Elling and the Bremen group—which is, you know, fair given my inability to reproduce anything near their concentrations via microwave extraction, but I digress—it would appear that there are two major zones of GDGT synthesis: between 300 and 800m as a wide swath below the photic zone with a second spike of located from 2150 to 2250m, at the top of the transition zone into the Orca Basin brine pool (Figure 8a,b). The peak in the upper water column is located farther below the surface than the 100 to 350m predominantly sub-photic zone range for planktonic thaumarchaeal production suggested by previous studies' measurements of abundance of archaeal cells, ammonia monooxygenase (*amoA*), 16S rRNA genes, and (Church et al., 2010; Francis et al., 2005; Santaro et al., 2010), though GDGT relative abundances through the Orca Basin water column are within normal range (Figure 8c,d; Table 2; Table 3). While crenarchaeol is by far the most abundant compound of the upper water column 0.2µm filter GDGTs, with an average GDGT-0 to crenarchaeol ratio ([0/Cren]) of 0.47 from the surface to 2100m depth, the bottom 200m exhibit [0/Cren] of 1.33, with an increase to 1.97 at 2220m depth and leveling off to roughly 1.35 in the brine pool proper (Figure 8c). The ratio of GDGT-1 to GDGT-0 ([1/0]) and GDGT-2 to GDGT-0 ([2/0]) decrease mirroring [Cren/0] (Figure 8d; Table 2). This follows the broader Atlantic trend of colder waters showing an increase in GDGT-0 relative to crenarchaeol (Pearson et al. 2016), given that temperature decreases generally with depth but increases through the transition into the brine pool (Figure 3a). Through the transition zone and the brine pool, the ratio of GDGT-1+2 to crenarchaeol [1+2/Cren] remains constant at 0.41 ± 0.06 but the difference in concentration of GDGT-1 and GDGT-2 does not. From 0 to 2100m, there is on average 0.5ng/L more GDGT-2 than GDGT-1; below there is 0.8ng/L less. Crossing over 2100m, [1/Cren] increases from 0.17 to 0.24, while the minor GDGTs in all other metrics decrease, [1/0] from 0.50 to 0.14; [2/Cren] from 0.24 to 0.18, and [2/0] from 0.34 to 0.19, suggesting an increase in GDGT-1 production but at a lesser scale than GDGT-0 (Table 2; Figure 8c,d).

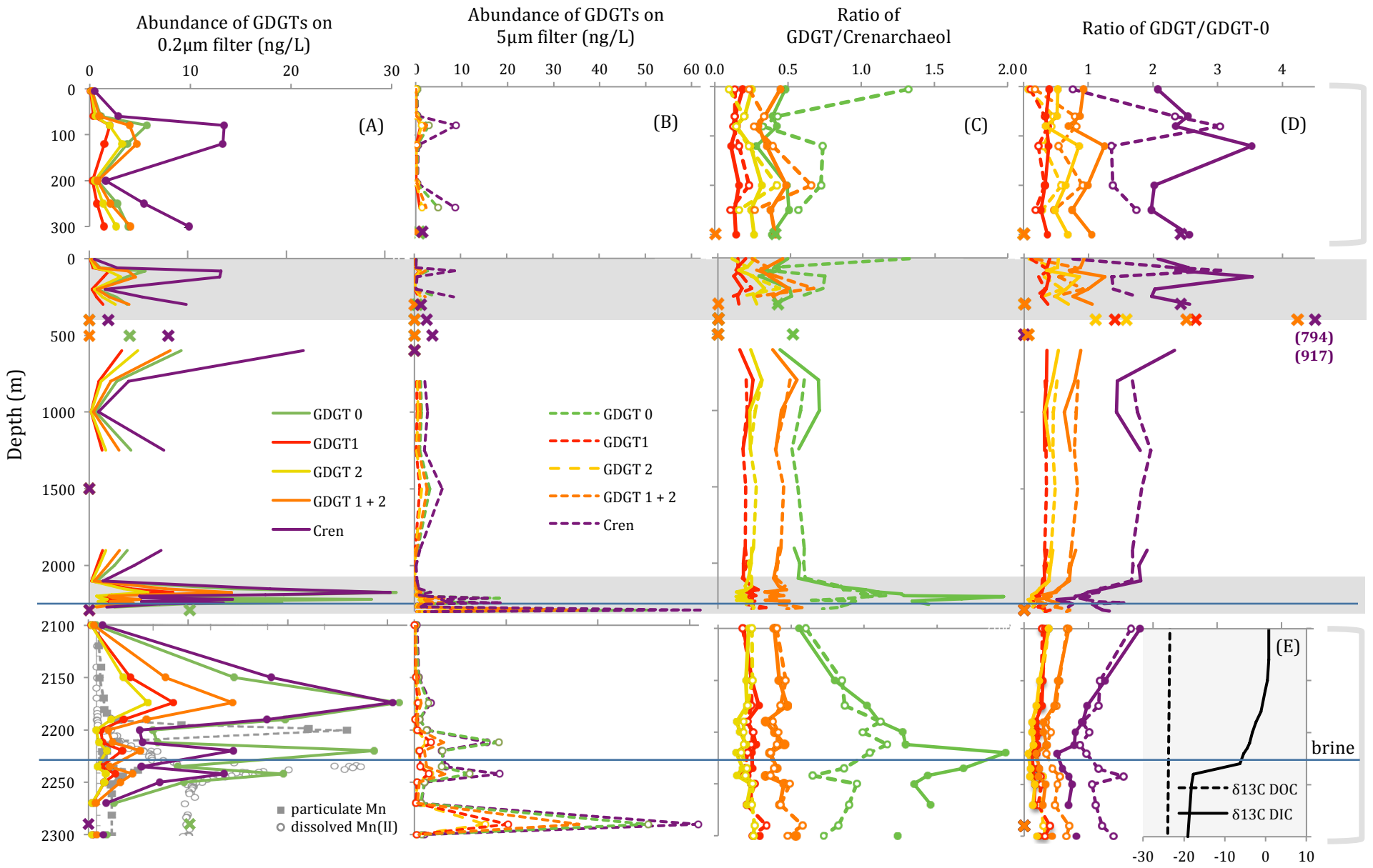

Figure 8: GDGT absolute and relative abundance in the Orca Basin water column. Three panels show a detail of 0-300m, the full 0 - 2300m water column, and a detail of the bottom 200m. The blue line marks the top of the brine pool transition zone (2230m). Solid lines and symbols represent GDGTs extracted from 0.2µm filters, dashed lines and open symbols the 5µm filter samples. GDGT-0 measurements are green, GDGT-1 red, GDGT-2 yellow, combined GDGT-1 and -2 orange, and crenarchaeol purple. Depths likely to be affected by collection or analytical errors are marked as an 'x'. Column (a) is abundance of GDGTs on 0.2µm filters and includes an underlay of particulate and dissolved Mn concentrations from Van Cappellen 1998; column (b) 5µm filter values. Column (c) presents [GDGT/Cren] ratio with depth and (d) the [GDGT/GDGT-0] ratio. Adapted from unpublished data with permission of Courtney Warren. DIC and DOC $\delta^{13}C$ are in inset (E), adapted from Shah et al. 2013.

There are noted differences in the abundance of GDGT moieties extracted from the 0.2µm and the 5µm filters (Figure 8a-d). The maximum water column values, excluding the brine pool, on the 0.2µm filter size occur at a depth of 600m, while the 5µm max occurs at 80m though this is difficult to compare as data from 300m and 400m as both the 0.2µm filters and 5µm filters appeared to be compromised by either collection, sampling, or analytical error, with 500m and 600m also compromised for 5µm (Table 1, Table 2). The most substantial distinctions between the two filter types occur in the bottommost 200m of collected water column samples. Abundances of GDGTs on the 0.2µm and 5µm filters alternate peaks and troughs at 2174m, 2200m, 2220m, 2235, and 2240m; the depths with elevated GDGTs on the 5µm filter (and decreased on the 0.2µm) correspond to the particular Mn spike at 2200m and particular Fe spikes at 2250 and 2280m (van Cappellen et al., 1998; Figure 3c,d; Figure 8a,b).

Without evoking secondary GDGT production at depth, the trends in water column abundance could be prescribed to preferential binding of crenarchaeol to Mn particulates which remain trapped at 2200m or even more so to iron particles that stagnate in the brine pool given the even greater reduction of [Cren/0] on the 0.2µm filters at depths 2220 through 2240. Chemocline filters with abundant particulate Mn and Fe may then yield greater relative abundances of GDGT-0 upon extraction as crenarchaeol is tighter bound to the metal compounds. Alternatively, there could be differential rates of GDGT-0 vs. crenarchaeol degradation given the acidity flux into the brine. Both of these mechanisms could be extended to explain graded behavior between crenarchaeol, GDGT-2, GDGT-1, and GDGT-0 if remineralization rate and adhesion to particulate matter are directly related to the number of rings. However, if either of these were the case and we assume that water column variation in GDGT abundances is related the release of GDGTs from whatever trapped them and dragged them down from closer to the surface and subsequent GDGT-hoarding and or destroying at depth, I would assume the relative abundance of GDGTs recovered from the sediment to preserve the signal of crenarchaeol loss and upwards of 40% of exported GDGTs to be GDGT-0 (Figure 5). An alternate case, which would explain a decrease in the proportion of GDGT-0 in sediments relative to the upper water column is if the extra GDGT-0 found at depth are the remain of sub-photic sources GDGTs preferentially stalling out and getting trapped above the brine.

In regards to preferential crenarchaeol dissolution with pH, yes, the doubling of [0/Cren] occurs over the pH bulge to –7.3 and then back to –7.8 of the peak at roughly 2180 to 2230 meters depth. There is a similar shift with the second acidity at around 2250m, but the [0/Cren] relationship is not well constrained or maintained through the rest of the brine where pH is considered constant (Table 2; Table 3). Preferential binding of crenarchaeol to particulate matter may be supported in the increase in [0/Cren] on the 0.2µm filter with a simultaneous decrease for the 5µm filter, but cannot explain why there would be increased [2/Cren] for both the 0.2µm and 5µm filter over the same interval. These two sin-synthesis scenarios also provide no clear mechanism for the carbon isotopic trends observed in the sediments, though it might be that I don't know of a process that would impart a differential isotopic fractionation on GDGT-0, GDGT-1+2, vs. GDGT-3, making all enriched in ^{13}C relative to an open marine setting, while the local DIC pool becomes light (Figure 3f, Figure 8.e).

I am instead inclined to prescribe the change in water column GDGT abundances to in-situ production at depth, not just because it's all more interesting that way. Production of GDGT-1, -2, and -0 in particularly have been noted across a broad swath of the archaeal tree of life (Schouten et al., 2013), and I find it unsurprising that archaea could be growing in a region that appears to support rampant biologically-mediated manganese cycling, iron reduction (van Cappellen et al., 1998), and potentially methanogenesis (Zhuang et al., 2014). If organisms similar to the ammonia oxidizing planktonic *Thaumarchaeota* live at above the brine pool, it may explain the sharp gradient in ammonia from 500µM in the brine to nigh 0 µM by 2200m depth if all the reduced, remineralized nitrogen escaping the brine is consumed (van Cappellen et al., 1998). Van Cappellen, though, signaled that ammonia concentration scaled with salt and would not require any biological mediation to achieve such levels. Whatever the metabolic system of the organisms involved, an additional source of GDGTs in a community of primarily autotrophic, GDGT-0 heavy producers explains both how relative abundances of GDGTs can change in the Orca Basin seawater / brine interface and provides a mechanism for enriching $\delta^{13}C_{GDGT}$ when $\delta^{13}C_{DIC}$ above the sediments is depleted. I evoke no assumptions about process other than part of the microbial community already known to exist above the Orca Basin brine pool produces GDGTs that are isotopically heavy via autotrophy and may be GDGT-0 heavy from the cold. Or just 'cuz diversity.

6.2 Seeing red? Maybe getting drowned by a brine pool…

We now assume that the majority of the Orca Basin sediment GDGTs are isotopically heavy in relation to published open-marine Atlantic values (Pearson et al., 2016) because of the addition of super-brine pool production. Logic would suggest then that the only valid explanation for why samples OB46.0cm and OB50.0cm yield values statistically identical to the open-marine Atlantic sites is because, at the time of sedimentation, those horizons were not deposited in contact with the brine pool (Figure 6c). Independent of isotopic clustering, though, this conclusion is also supported by sedimentological observations and basic redox chemistry.

As part of 1999 study reporting on anomalous enrichments of iron monosulfide in euxinic marine sediments, Hurtgen et al. provided descriptions of four box cores were collected in and around the Orca Basin. Three box cores were collected at anoxic sites, one on the medial saddle and two from the deep portion of the southern sub-basin, and consisted entirely of black microlaminated mud. The last box core was from where the water-column redox transition (chemocline) impinges with the basin margin at 2240m; the upper 43.5cm are described as "exhibit[ing] exhibit a dramatic brick red color mottled with light-gray mud" with a unit of light-gray mud to the base of the subcore 8.5cm below. The two piston cores were collected along the basin margin, under an oxic water column, and contain water-rich, homogenized, bioturbated muds ranging from olive-brown and reddish browns towards surface and gray horizons lower down.

The three sections of core OB-0412-MC-0502C sampled in this study, with a unit of homogenized grey muds including a number of thick red (28 to 56cm) bands bookended by finely bedded black and gray mud (0 to 28cm, 56 to 70cm) would correlate respectively with sedimentation at depths characterized by either chemocline or sub-oxic water column conditions for the medial interval and placement under the anoxic-brine given characteristics described by Hurtgen et al., 1999. These observations also make sense given geochemical and sedimentological processes. Under the influence of the strong stratification of the transition zone acting as a particle trap and anoxia of the brine, we would expect to find thinly laminated sediments, well defined by both slow rates of deposition and a lack of bioturbation, the black coloration a likely byproduct of sulfides produced

in the anoxic environment. The red banding shows promise as a great marker of chemocline depth, as it may well represent the oxidation of reduced iron inherited from brine brought into contact with an oxygenated environment, and would therefore shift in lateral extent during the retraction and expansion of the brine pool. The lack of clear banding in the gray sediments positioned between red chemocline layers in intermediate core depths could then represent initiation of bioturbation with the oxygenation of the surface sediments.

My stratigraphic interpretation requires the Orca Basin brine dissolved Fe(II) profile to remain in a similar state through the entire time interval 70cm of sediment deposition reflects in core OB-0412-MC-0502C (Figure 3d), as well as a contraction and expansion of the brine to be feasible within such a time window. Radiocarbon analysis suggests that the Orca Basin DIC reservoir have been stable over the past 8,000 years (Shah et al., 2013) and attests to continuous deposition of rates upwards of 35cm/kyr (Flower et al., 2011). Analytical measurements have provided consistent brine composition over a thirty year time period (Shah et al., 2013; Shokes et al., 1977); red banding in Orca Basin sediments could then be attributed as a marker of chemocline depth in this study if elevated dissolved Fe(II) load has been maintained in the brine for the past 2,000 years. Because the Orca Basin brine is sourced not in-situ but through lateral advection of brine produced by the dissolution of a nearby salt exposure (Pilcher and Blumstein, 2007; Shokes et al., 1977), this provides both a foundation for assuming consistency of brine composition as well as a mechanism for fluctuation in brine volume and expanse at such time scales.

It is likely that shifts in the structure of the water column overlaying core OB-0412-MC-0502C would be accompanied by changes in the absolute rate of sediment accumulation. The absolute amount of GDGTs exported per unit time may change based on the current depth of the seawater-brine transition zone, as may the amount of time each 0.5cm slice of the core represents. However, if GDGTs are primarily exported from the upper water column to the sediment by association with larger particles, the mass of GDGTs produce in surface waters and extracted for this study relative to the mass of sediment deposited and sampled, i.e. μg GDGT/g sediment, should not change if water column GDGT production is constant. The shift in this ratio between brine and non-brine Orca Basin horizons may then quantify production of GDGTs at depth.

Table 4:
Summary of Atlantic Ocean carbon isotopic trends

Site Type	Brine Pool	Open Marine			Δ brine to
Region	Orca Basin	Orca Basin	Atlantic	Combined	open marine
$\delta^{13}C$ of GDGTs					
GDGT-0	−18.2±0.1	−19.3±0.2	−19.4±0.2	−19.4±0.2	−1.2
GDGT-1	−18.4±0.0		−20.4±0.2		−2.0
GDGT-1+2	−18.6±0.2	−19.5±0.0	−20.1±0.5	−19.8±0.6	−1.2
GDGT-2	−18.8±0.0		−19.9±0.6		−1.1
Crenarchaeol	−18.4±0.2	−18.7±0.1	−18.9±0.2	−18.8±0.1	−0.4
$\Delta^{13}C$ of GDGTs					
GDGT- 0/1	−0.2		−1.0		
GDGT-0/1+2	−0.4	−0.2	−0.7	−0.4	0.2
GDGT-0/2	−0.6		−0.5		
GDGT-0/Cren	−0.2	0.6	0.5	0.6	0.8

6.3 Patterns of Atlantic GDGT signals in and out of the brine

Separating the Orca Basin samples into two bins based on sedimentology, GDGT abundance, and $\delta^{13}C_{GDGT}$ values pairs horizons OB46.0cm and OB50.0cm as the open marine sites and clusters horizons OB0.5cm, OB4.0cm, OB8.5cm, OB15.5cm, OB22.0cm, OB26.0cm, and OB64.0cm as the brine pool delegation (Table 1; Figure 6a-c). The determination of OB46.0cm and OB50.0cm as open marine is supported by GDGT-0 and crenarchaeol carbon isotopic compositions statistically identical to those of the open marine Atlantic sites measured in Pearson et al. 2016 (Figure 6c, Table 4). GDGT-1 and GDGT-2 from Orca Basin on average are distinctly heavier than those produced in the other Atlantic sites, though do fall within 1σ of the greater Atlantic values.

Differences between the absolute value of $\delta^{13}C_{GDGT}$ between environments as well as changes in the isotopic offset between compounds mark a drastically different ecology dominating the signal produced in brine pool as opposed to open marine conditions. GDGT-0 and GDGT-1+2 are both 1.2‰ depleted in open marine samples relative to the brine; Crenarchaeol is only depleted by 0.5‰. For the brine pool sites, GDGT-2 is more depleted than GDGT-1, while the reverse is true

at the Atlantic sites measured in Pearson et al. 2016, though sample size is small with only 2 GDGT-1 measurements and 3 for GDGT-1, and isotopic values for both from the Carolina Margin site. Regardless, orca basin marine sites show a smaller offset between GDGT-0 and GDGT-1 and -2 combined than the brine localities. Most marked is the change in sign of the relationship between GDGT-0 and crenarchaeol, with crenarchaeol 0.2‰ lighter within the brine pool yet heavier than GDGT-0 by 0.6‰ in all other Atlantic sites (Table 4). In total these findings suggest that the GDGTs exported into the Orca Basin sedimentary record under brine pool conditions are greatly influenced by autotrophic production at depth. Given that the effect of this additional source is felt greatest in the composition of GDGT-0, then GDGT-1, then GDGT-2, and least by crenarchaeol, this supports conclusions drawn from water column abundance data set that the organisms producing GDGTs in the brine-pool transition zone are preferentially adding GDGT-0, and to a lesser extent GDGT-1 and GDGT-2 to the total export pool. The relative decrease in GDGT-2 material when the brine pool retracted, exposing core OB-0412-MC-0502C to oxic conditions, can partially explain the reduction in isotopic offset between GDGT-0 and GDGT-1+2 for these horizons, visualized in Figure 6a. There may also be a $\Delta^{13}C_{0/1+2}$ shift in GDGTs produced in the upper water column vs. depth, signaling alternative bio-synthetic pathways for GDGTs and the potential for GDGTs to be produced from organisms with much wider variety in habitat, form, and even enzymatic composition than taken for granted in the GDGT literature (Lincoln et al., 2014; Schouten et al. 2013; Tierney 2014).

6.4 Isotope mass balance and $\delta^{13}C$ of GDGTs produced in the transition zone

The carbon isotopic composition of GDGTs in Orca Basin sediments lend to a two-end member isotope mass balance mixing model of Atlantic marine GDGTs and seawater-brine pool transition zone production:

$$\delta_{brine} = f_{marine}\delta_{marine} + (1 - f_{marine})\delta_{TZ} \quad (1)$$

The carbon isotopic composition of brine pool samples (δ_{BRINE}) and the marine signal (δ_{MARINE}) are known from SWiM-IRMS, with brine pool sediment $\delta^{13}C$ compositions of –18.2‰ for GDGT-0, –18.6‰ for GDGT-1+2, and –18.4‰ for crenarchaeol, and marine values of –19.8‰ for

Table 5:
Estimating $\delta^{13}C$ for seawater-brine transition zone sourced GDGTs

	$\delta^{13}C$ (‰)		μg GDGT/g sediment		f_{MARINE}	$\delta^{13}C_{TZ}$ (‰)	
	brine	marine	brine	marine		range	average
GDGT-0	-18.2	-19.4	1.58±0.41	0.43±0.03	20-30%	-17.4 to -17.9	-17.6
GDGT-1+2	-18.6	-19.5	1.89±0.65	0.48±0.08	16-46%	-17.9 to -18.5	–18.2
Crenarchaeol	-18.4	-18.8	4.01±0.76	1.12±0.13	21-39%	-18.2 to -18.3	-18.2

GDGT-0 from all Atlantic sites, –19.5‰ for GDGT-1+2 in the Orca Basin (–19.8‰ at all sites), and –18.8±0.1‰ for crenarchaeol) (Table 4). I estimate the fraction of marine input (f_{MARINE}) as the relative abundance of GDGT per gram sediment in the open marine Orca Basin horizons and abundance of GDGT pre gram sediment in the depths associated with sub-brine pool deposition. This metric is of much lower precision than isotopic measurements; variations in ASE extraction and chromatography efficiency have a heightened potential to alter the absolute value of lipids recovered. However, if we take these values to be representative of an actual phenomenon, only roughly 20-40% of GDGTs collected from brine pool sediments were produced in the upper water column (Table 1). This leaves us with one equation and one unknown, the carbon isotopic composition of GDGTs produced below 2100m depth (δ_{TZ}).

The carbon isotopic composition of the GDGTs produced in the transition zone are calculated to be –17.6‰ for GDGT-0, –18.2‰ for GDGT-1+2, and –18.2‰ for crenarchaeol (Table 5). The value of δ_{TZ} for crenarchaeol is then 0.6‰ heavier than the bulk Atlantic, GDGT-1+2 1.3‰ heavier, and GDGT-0 1.8‰. My GDGT-0 δ_{TZ} value matches that of the theoretical carbon isotopic fractionation εDIC/GDGT of strictly autotrophic Atlantic GDGTs, –17.5±0.4‰, (Pearson et al., 2016), suggesting the brine dwellers, or at least the organisms at depth contributing the greatest isotopic fractionation on $\delta^{13}C_{GDGT\text{-}0}$, are almost entirely autotrophic and could therefore serve as a reservoir tracking marine $\delta^{13}C_{DIC}$.

As an experimental calculation, and an additional layer of abstraction, I also evaluated the isotopic composition of the transition zone ($\delta^{13}C_{TZ}$) as a two-part mixture of *Thaumarchaeota*, or at least the same organisms as present in the upper water column, and *Euryarcheota*, or just some other

Table 6:
Breaking down $\delta^{13}C_{TZ}$ to a standard Atlantic and 'other' isotopic signal

	$\delta^{13}C_{TZ}$	$\delta^{13}C_{MARINE}$	f_{MARINE}	$\delta^{13}C_{OTHER}$
GDGT-0	-17.6	-19.4	0.47	-16.0
GDGT-1+2	-18.2	-19.5	0.63	-15.9
Crenarchaeol	-18.2	-18.8	0.61	-17.3

exogenous source. A mixed source of GDGTs is suggested from the $\Delta^{13}C_{GDGT}$ record, as GDGT-0 expresses the greatest divergence in transition zone and open marine $\delta^{13}C$ values and yet crenarchaeol, long considered to be compound synthesized by the most phylogenetically restricted group (Schouten et al., 2013), is relatively unchanged. The these two groups may actually be represented distinctly in the water column GDGT abundance data, as [0/Cren] from the 0.2µm filter smoothly increases from 2100 to 2220m yet then decreases into the brine (Figure 8c) and ergo not directly related to the coincident changes in temperature (Figure 3a). We have a massive peak in GDGT abundance with a [0/Cren] ration of ~1 at 2175m, a peak with [0/Cren] or ~2 at 2220m, and a third peak at 2250m with [0/Cren] of ~1.4 (Figure 8a,c), suggesting a trimodal distribution aligned with purported zones of manganese oxidation and iron reduction (van Cappellen et al., 1998). For this simplified and simplistic model, I suggest that the 2175m peak corresponds to organisms similar to the broader marine community, as there is the potential for ammonia oxidation and lower [0/Cren] at this depth, and lump together all other productivity as 'other'. This calculation was done with a modified version of equation (1):

$$\delta_{TZ} = f_{marine}\delta_{marine} + (1 - f_{marine})\delta_{other} \quad (2)$$

The value of f_{MARINE} is calculated as a very naïve summation of the ng/L of GDGTs collected from depths 2150 to 2200 representing marine-type input, and depths 2212 to 2250m other. This results in an 'other' sources with isotopic compositions of GDGT-0 at –16.0, GDGT-1+2 at –15.9, and crenarchaeol at –17.3‰ (Table 6). Here crenarchaeol is the compound with an isotopic composition curiously similar the hypothesized $\delta^{13}C$ composition of autotrophic GDGT, the compound Pearson et al. (2016) suggest as a possible $\delta^{13}C_{DIC}$ tracer.

6.5 Paleoceanographic implications – TEX_{86} and $\delta^{13}C_{DIC}$

The identification of a zone of primarily autotrophic GDGT production above the Orca Basin brine pool presents broad repercussions for the field of paleoclimatology. In the realm of TEX_{86} and sea surface temperature reconstruction, the existence of a bottom water GDGT-synthesizing community associated with a strong salinity gradient could explain why Red Sea TEX_{86} calculations always yield lower sea surface temperature than calibrations would predict (Elling et al., 2015; Kim et al., 2010; Trommer et al., 2009). The transition zone community in Orca Basin may most noticeably increase the relative abundance of GDGT-0 (Figure 8), but there is also a significant shift in the abundance of GDGT-1 and GDGT-2 in relation to crenarchaeol (Table 3, Figure 8c). The impact of an increase in [1/Cren] relative to [2/Cren] is immediately apparent from the construction of the TEX_{86} SST proxy:

$$\mathrm{TEX}_{86} = \frac{[\mathrm{GDGT}-2] + [\mathrm{GDGT}-3] + [\mathrm{Cren}']}{[\mathrm{GDGT}-1] + [\mathrm{GDGT}-2] + [\mathrm{GDGT}-3] + [\mathrm{Cren}']} \quad (3)$$

$$\mathrm{SST} = 56.2 \times \mathrm{TEX}_{86} - 10.8 \quad (4)$$

The contribution of additional GDGT-1 from depth will decrease the value of TEX_{86} and any subsequent sea surface temperature reconstructions. This phenomenon can be observed in SST reconstructions from relative GDGT abundances in the Orca Basin water column, where TEX_{86} predicts SST values of 26 – 31°C from GDGTs collected from 5 to 2100m depth but 14 – 25° for those 2150m and below (Table 7; Table 8).

The isotopic composition of the Orca Basin sediment GDGTs also presents a significant challenge to the longstanding endeavor to use $\delta^{13}C$ of GDGTs or archaeal biphytanes as a paleo-$\delta^{13}C_{DIC}$ proxy. The theory behind a GDGT/DIC relationship was proposed in the late 1990s under the assumption that GDGTs preserved in the rock/mud record are predominantly derived from autotrophic, planktonic export (Hoefs et al, 1997; Schouten et al., 1998). The method has previously been used on archaeal biphytanes to infer the isotopic composition of dissolved

Table 7:

GDGT Proxies and Orca Basin 0.2μm Filters

Depth (m)	TEX86 [a]	TEX_{86} SST (°C) [b]	TEX_{86}^{H} SST (°C) [c]	Methane Index [d]	GDGT-0/Cren	Ring Index [e]	RI_{TEX} [e]
5	0.70	28.19	28.79	0.31	0.48	2.85	2.69
60	0.72	28.91	29.76	0.29	0.39	14.46	2.76
80	0.65	25.73	25.64	0.26	0.43	65.43	2.49
120	0.78	31.10	32.86	0.25	0.28	68.14	3.00
200	0.76	30.31	31.71	0.30	0.49	9.00	2.91
250	0.73	29.40	30.43	0.27	0.51	27.79	2.81
300	0.74	29.59	30.69	0.28	0.39	51.37	2.83
400†	0.99	38.32	44.88	0.02	0.00	8.96	4.09
500†	1.00	38.51	45.23	0.02	0.52	35.58	4.12
600	0.74	29.64	30.77	0.25	0.43	117.43	2.84
800	0.69	27.56	27.96	0.32	0.69	23.12	2.64
1000	0.66	26.16	26.17	0.27	0.70	5.04	2.52
1250	0.66	26.35	26.41	0.27	0.56	38.42	2.54
1500†						0.00	
1900	0.65	25.81	25.74	0.29	0.53	37.09	2.49
2000	0.67	26.49	26.59	0.28	0.56	23.21	2.55
2100	0.66	26.04	26.02	0.27	0.55	7.09	2.51
2150	0.54	20.07	19.32	0.29	0.80	89.98	2.13
2175	0.47	16.31	15.74	0.32	1.02	148.81	1.97
2190	0.46	15.53	15.05	0.25	1.11	82.22	1.94
2200	0.46	15.52	15.04	0.28	1.26	24.24	1.94
2212	0.59	22.97	22.40	0.30	1.29	28.80	2.29
2220	0.43	13.72	13.52	0.26	1.97	67.97	1.88
2235	0.51	18.31	17.59	0.29	1.68	25.77	2.05
2242	0.50	17.84	17.14	0.25	1.43	64.10	2.03
2250	0.60	23.36	22.85	0.32	1.34	36.12	2.32
2270	0.62	24.57	24.25	0.28	1.46	9.38	2.40
2290†						0.00	
2300	0.48	17.01	16.37	0.36	1.23	7.26	1.99

† suspect depths (Table 2)_ [a] Schouten et al. 2002 [b] Kim et al. 2008 [c] Kim et al. 2010 [d] Zhang et al. 2011 [e] Zhang et al. 2016

Table 8:

GDGT-0 Proxies and Orca Basin 5µm Filters

Depth (m)	TEX86 [a]	TEX_{86} SST (°C) [b]	TEX_{86}^{H} SST (°C) [c]	Methane Index [d]	GDGT-0/Cren	Ring Index [e]	RI_{TEX} [e]
5	0.69	27.77	28.23	0.16	1.32	1.68	2.66
60	0.77	30.99	32.69	0.25	0.43	2.20	2.98
80	0.67	26.83	27.01	0.24	0.33	41.97	2.57
120	0.74	29.79	30.97	0.24	0.74	3.05	2.85
200	0.75	30.17	31.52	0.36	0.72	2.31	2.89
250	0.71	28.61	29.36	0.21	0.57	40.98	2.73
300§	0.99	38.25	44.74	0.03	0.41	6.66	4.07
400§	0.98	37.99	44.26	0.02	0.00	12.18	4.02
500§	1.00	38.50	45.21	0.02	0.00	17.56	4.12
600§						0.00	
800	0.76	30.48	31.96	0.28	0.60	13.36	2.93
1000	0.66	26.47	26.56	0.30	0.57	14.72	2.55
1250	0.68	27.10	27.36	0.27	0.51	11.37	2.60
1500	0.72	28.82	29.64	0.28	0.55	33.89	2.75
1900	0.70	28.11	28.69	0.28	0.60	6.39	2.69
2000	0.72	28.95	29.81	0.24	0.59	2.25	2.77
2100	0.69	27.72	28.16	0.28	0.60	2.81	2.65
2150	0.71	28.29	28.92	0.27	0.85	5.82	2.70
2175	0.59	22.82	22.24	0.29	0.87	17.98	2.28
2190	0.63	24.67	24.37	0.26	1.11	5.68	2.41
2200	0.54	20.57	19.83	0.28	0.99	13.73	2.16
2212	0.58	22.22	21.57	0.27	1.16	80.68	2.25
2220	0.58	22.33	21.70	0.25	1.04	29.55	2.25
2235	0.61	23.98	23.56	0.27	0.87	34.13	2.36
2242	0.62	24.41	24.05	0.26	0.65	90.95	2.39
2250	0.60	23.33	22.81	0.30	0.95	11.97	2.32
2270	0.73	29.28	30.27	0.26	0.90	8.66	2.80
2290	0.60	23.33	22.81	0.33	0.82	357.55	2.32
2300	0.67	26.82	27.00	0.29	0.72	12.05	2.57

§ suspect depths (Table 3)_ [a] Schouten et al. 2002 [b] Kim et al. 2008 [c] Kim et al. 2010 [d] Zhang et al. 2011 [e] Zhang et al. 2016

inorganic carbon during the Cretaceous ocean anoxic events (Kuypers et al., 2001). More recently, a method of reconstructing $\delta^{13}C_{DIC}$ from the isotopic composition of isolated crenarchaeol has been suggested under the observations that crenarchaeol in their data set contained the lowest fraction of exogenous material (equivalent to [1 – f_{MARINE}] in equation (1) and crenarchaeol is likely to be produced by a community less variable in the relative contribution of heterotrophy vs. mixotrophy (Pearson et al., 2016). The isotopic composition crenarchaeol from the two Orca Basin sediment samples assumed to be deposited under an oxic water column are identical to those reported by Pearson et al. for their Atlantic sites, bolstering the prospect of using $\delta^{13}C_{Cren}$ to reconstruct $\delta^{13}C_{DIC}$ for locations dominated by marine planktonic input. It may also be of significance that my hastily calculated $\delta^{13}C_{OTHER}$ for crenarchaeol would suggest the existence of a purely autotrophic GDGT-0 producer with a $\delta^{13}C_{Cren}$ value of –17.3‰.

This would seem a great breakthrough in providing a means to measure $\delta^{13}C_{DIC}$ for localities in which carbonates are absent or diagenetically altered. However, my measurements for Orca Basin brine-associated sediments, the exact kind of facies for which a lipid-based DIC proxy would be most useful, would suggest that instead of measured compound specific GDGT ^{13}C tracking DIC composition, it moves in the opposite directions (Figure 3f; Figure 6a). My isotopically lightest $\delta^{13}C_{GDGT}$ values were obtained from the sediments laid down when the brine pool retracted and no longer covered the core, whereas $\delta^{13}C_{GDGT}$ was significantly more enriched in ^{13}C when under the influence of the greatly $\delta^{13}C_{DIC}$ depleted brine (Table 1). For one, this concurs with Pearson et al.'s conclusion that the crenarchaeol-based proxy system is unlikely to work in basinal settings. It also suggests that the fractionation of GDGT-0 from DIC εDIC/GDGT in the transition zone community is even less than the estimated value of $\delta^{13}C_{TZ}$ of –17.6‰ (Table 5) as $\delta^{13}C_{DIC}$ decreases from 1‰ to –6‰ from depths 2100 to 2230m (Shah et al., 2013; Figure 3f), then an unquestionably autotrophic signature (Pearson et al., 2016). It may then be the case that the isotopic composition of GDGT-0 (or the composition of non-*Thaumarchaeota* crenarchaeol as computed by equation (2)) recovered from basins with highly stratified, euxinic bottom water conditions—such as the case in the Orca Basin or Cretaceous anoxic events—incorporates a direct measurement of paleo-$\delta^{13}C_{DIC}$.

6.6 Potential for new proxy systems using $\Delta^{13}C_{Cren/0}$, $\Delta^{13}C_{1+2/0}$ and $\Delta^{13}C_{GDGT\text{-}0}$

I would now like to propose frameworks for two new GDGT-based proxy systems that could aid in (1) the identification of sites with benthic or terrestrial GDGT production to be excluded from calibration studies or paleoceanography reconstructions and (2) establishing a means to reconstruct the past isotopic composition of marine dissolved inorganic carbon independent of the precipitation and preservation of carbonates.

The two Orca Basin sediment horizons I have identified as being deposited outside of the brine pool exhibit identical $\delta^{13}C_{GDGT\text{-}0}$ and $\delta^{13}C_{Cren}$ values within SWiM-IRMS analytical error as all previously reported open Atlantic sites (Figure 6c; Table 4). This also means that $\Delta^{13}C_{Cren/0}$ appears to be constant at –0.6‰ for upper water-column GDGT production throughout the North Atlantic Ocean, given the $\delta^{13}C_{GDGT}$ values were obtained from sites spanning 10° to 43°N and 60° to 91°W (Pearson et al. 2016). The carbon isotopic values obtained from horizons where Orca Basin core OB-0412-MC-0502C was located within the extent of the brine pool are equally self-similar, but $\Delta^{13}C_{Cren/0}$ is instead 0.2‰ due to autotrophic production of GDGT-0 in excess to crenarchaeol at depth. Given these results, I propose that TEX_{86} etc. overprinting by exogenous autotrophic production can be identified in sediment GDGTs from measuring $\Delta^{13}C_{Cren/0}$, using –0.6‰ as a base value for open-marine production, at least for the Atlantic.

The presence of an offset between $\delta^{13}C_{GDGT\text{-}0}$ and $\delta^{13}C_{GDGT\text{-}1+2}$ instead seems to correlate with the potential for multi-source input. Values of $\Delta^{13}C_{1+2/0}$ greater than analytical precision only occur at the near shore Carolina Margin site, NAtl4 off the Gulf of St. Lawrence, the brine pool Orca Basin depths, and my calculations for transition zone GDGT composition (Pearson et al., 2016; Figure 6c; Table 5). Open marine Orca Basin horizons, NAtl11, and my theoretical non-*Thaumarchaeota* 'other' source of GDGTs in the transition zone all exhibit isotopic values of GDGT-1 and GDGT-2 no different than GDGT-0 (Figure 6c; Table 6).

The amplitude of offset between $\delta^{13}C_{GDGT\text{-}0}$ values for horizons inside and out of the brine pool (including non Orca Basin sites) is also notable, given the constant Orca Basin $\Delta^{13}C_{GDGT\text{-}0}$ value of

–1.2‰ and the resulting $\delta^{13}C_{TZ}$ computation of –17.6‰ signaling that the non-planktonic GDGT-0 input is purely autotrophic in nature (Table 4; Table 5). The offset of brine pool and marine $\delta^{13}C_{GDGT-1+2}$ is also –1.2‰ when including all marine Atlantic sites, but decreases to –0.9‰ when only considering the offset between Orca Basin samples; $\Delta^{13}C_{Cren}$ between brine pool and marine values is the smallest at only –0.4‰ (Table 4). This suggests that the bulk community producing GDGTs at depth effects a total fractions quite distinct from the general marine community. These shifts in Orca Basin appear to be explainable by the existence of two groups of GDGT synthesizers at depth: one exhibiting the same degree of mixotrophy and fractionation as open marine *Thaumarchaeota* (though potentially oxidizing manganese instead of ammonia), producing GDGTs with isotopic value the same as those sourced from the upper surface water that produce most of the brine pool in-situ crenarchaeol and a second obligate autotrophic group with that corresponds to zones of iron reduction (van Cappellen et al., 1998; Table 6). But in all a back calculation based of $\Delta^{13}C_{GDGT-0}$ between a restricted basin and open marine setting, with some controls on the fraction of GDGTs sources from the upper water column to get $\delta^{13}C_{GDGT-0}$ of the exogenous tetraethers could prove to serve as a paleo-$\delta^{13}C_{DIC}$ proxy, with $\Delta^{13}C_{Cren/0}$ and $\Delta^{13}C_{1+2/0}$providing a metric by which to classify sites as marine and basinal settings which can be used both through space and time.

The conceptual framework developed around $\Delta^{13}C_{Cren/0}$, $\Delta^{13}C_{1+2/0}$ and $\Delta^{13}C_{GDGT-0}$ may be able to explain some be some of the isotopic variation Pearson et al. noted at their Pacific sites (Figure 9) as opposed to the very consistent Atlantic (Figure 6c). First, almost all of the Pacific measurements

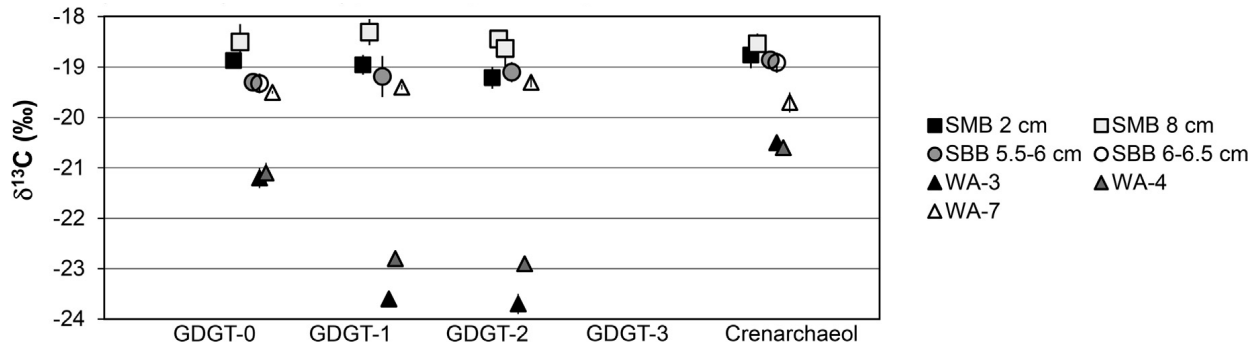

Figure 9: $\delta^{13}C_{GDGT}$ values for Pacific Sites. Adapted from Pearson et al 2016.

are from basinal settings: two horizons in the Santa Monica Basin (SMB), two in the Santa Barbara Basin (SBB) and a sample collected at 2589m depth along the Washington Margin (WA-7). These 5 sites all exhibit a shoaling or inversion of $\Delta^{13}C_{Cren/0}$ signaling the potential for autotrophic GDGT production, while the upper Washington Margin samples (WA-3 and WA-4) exhibit the same value as all Atlantic open marine sites (–0.6‰) though offset by an absolute value of ~0.2‰. Comparison of $\Delta^{13}C_{1+2/0}$ would indicate a large amount of light, terrestrially sourced GDGT-1 and GDGT-2 similar to the Atlantic Carolina Margin and NAtl4 (Figure 6c; Figure 9) whereas SMB and SBB, located by low rain and potentially low terrestrial runoff L.A., shows little to no fractionation, though this difference is not noted in the BIT Index.. The near shore Washington Margin sites exhibit a fractionation of almost –2‰.The relationship between WA-7 and partner up-slope sites WA-3 and WA-4 GDGT-0 and crenarchaeol seems to mirror that of the brine and marine Orca Basin samples, with $\Delta^{13}C_{Cren}$ noticeably smaller than $\Delta^{13}C_{Cren}$. GDGT production at depth for this site similar to that at the Orca Basin under brine pool conditions could explain this offset, with a Pacific autotrophic $\delta^{13}C_{GDGT\text{-}0}$ value calculated for the exogenous material if marine GDGT-0 with isotopic composition of WA-3 and WA-4 comprises 30% of burial at WA-7 (Figure 9). Water column profile data and additional information about local drainage at the Pacific sites would further aid in either supporting or disproving these proposed proxies.

6.7 Orca Basin and other GDGT proxy systems

Outside of exploring the isotopic composition of GDGTs exported to the sediments, the Orca Basin water column GDGT abundance data set can be used to evaluate how other GDGT proxy systems relate to the actual production and accumulation of GDGTs through the water column, as discussed in regards to TEX_{86} in section 6.5, and will now be briefly explored in relation to the Methane Index and Ring Index. The methane index was proposed to quantify the relative contribution of methanotrophic *Euryarchaeota* to the sediment GDGT pool (assuming GDGT-1, -2, and -3 to be representative of *Euryarchaeota*), and is calculated as:

$$MI = \frac{[GDGT-1] + [GDGT-2] + [GDGT-3]}{[GDGT-1] + [GDGT-1] + [GDGT-3] + [Crenarchaeol] + [Cren-isomer]} \quad (5)$$

While the methane index yields values of 0.28±0.03 throughout the whole water column, there are slightly elevated values at depths 2212, 2235, and 2250m (i.e. 0.30, 0.29, and 0.32 as compared to intervening values of 0.26 and 0.25) that correlated to depths of the first peak in benthic GDGT-0 production (Figure 8a), and then the peak of dissolved Mn (II) (Figure 3c), and the peak in and rapid drop in particulate iron (Figure 3d). While the presence of 16S rRNA sequences of the halophilic, methylotophic archaeal genus *Methanohalophilu* have been reported in the southern orca basin (Zhuang et al., 2014), I find it unlikely that this small signal is driven by methanogens living at depths of known manganese oxidation and iron reduction (van Cappellen et al., 1998) given the low energy potential of methanogenesis and that isotopic values of GDGTs become enriched in ^{13}C through the brine, not depleted as would be incurred by methanogenesis.

There have been a multitude of ring indices proposed over the years relating various factors to the average number of rings in extracted total GDGT (Schouten et al., 2013). The most recent is:

$$\mathrm{RI} = 0\times[\mathrm{GDGT}-0] + 1\times[\mathrm{GDGT}-1] + 2\times[\mathrm{GDGT}-2] + 3\times[\mathrm{GDGT}-3] + 4\times[\mathrm{Cren}] + 4\times[\mathrm{Cren}'] \quad (6)$$

to determine if TEX_{86} temperature estimates are influenced by non-thermal factors (Zhang et al., 2016). When RI and TEX_{86} indices from sediment records deviate from the modern global calibration for TEX_{86}/RI, TEX_{86} based temperature reconstructions should be considered questionable. TEX_{86} at all depths in the water column would predict a RI_{TEX} value lower than the calculated ring average, but the ΔRI for 5 to 2100m is 0.67±0.17 for 0.2µm filter and 0.65±0.18 for the 5µm filters, and ΔRI for 2150 to 2300m is 1.19±0.19 for 0.2µm filter and 0.91±0.18 for 5µm filter (Table 7; Table 8). These values seem to suggest that biosynthesis at all depths is influenced by nonthermal effects, as they exceed the 95% confidence interval established to be ±0.3, but also that the GDGTs collected 0.2µm and 5µm filter in the upper water column are effected similarly where as the 0.2µm filter GDGTs, or samples more representative of in-situ production, are greater influenced by non thermal or methanogenic factors than those on the larger filter fraction. This metric supports the general conclusion that there is GDGT synthesis at depth by organisms with differences in metabolic processes than the GDGT-producers higher in the water column.

6.8 Future directions

6.8.1: Orca Basin water column samples

The data set I acquired from Felix Elling, Courtney Warren, and their collaborators is ripe for the picking. While my analysis was largely limited to examining the relative abundance of GDGT moieties with depth, closer study and additional work evaluating how TEX_{86} calibrations, Ring Index parameters, Methane Index, relative abundance of GDGTs, and geochemical gradients change with depth could prove instrumental in understanding how the ecology of GDGTs producers shifts with depths. Future focus on GDGT-3, GDGT-4, and the crenarchaeol isomer, though lacking in companion $\delta^{13}C$ data, is crucial as those are the moieties often assigned the most informational value in proxy systems. Further monitoring of how GDGT proxies skew within the anoxic, hypersaline brine and seawater-brine transition zone, especially in a location with purported methanogenesis in the deep and extensive manganese oxidation at and above the interface (Zhuang et al., 2014; van Cappellen et al., 1998), could yield insight into alternative metabolisms that underlie the synthesis of GDGTs. Investigation into more effective and efficient lipid extraction methods for the plastic Durapore and Nitex filters used in this cruise may allow for compound specific $\delta^{13}C$ measurements of water column GDGT. This would be a boon in many ways additional to simply being able to easily extract lipids from plastic. Water column $\delta^{13}C_{GDGT}$ would aid in precisely determining the sourcing of sediment GDGTs, and potentially characterize a fundamental difference between GDGTs produced by *Thaumarchaeota* et al. in the upper water column and the GDGT-0 heavy, proposed in-situ signal I predict from the Orca Basin carbon isotopic record (Table 5; Table 6).

6.8.2: Orca Basin sediment cores

The next immediate step to fill out this study is to get relative abundance data of all GDGTs from the Orca Basin to be able to compare sediment values for proxies like TEX_{86} (Kim et al., 2010) and the Ring Index (Zhang et al., 2016) to the greater water column profile. If I can verify that the brine pool samples exhibiting altered $\Delta^{13}C_{Cren/0,}$ $\Delta^{13}C_{1+2/0}$ and $\Delta^{13}C_{GDGT\text{-}0}$ are also projected to be

compromised via other metrics, this can further support my hypotheses that specific trends in carbon isotopic values may be used for quantitative reconstruction of past environmental variables.

In regards to the pursuit of measuring compound-specific carbon isotopic composition of GDGTs, the next logical step from here would be to run SWiM-IRMS on larger samples sizes such that it is possible to obtain a greater number of individual measurements for GDGT-1 and GDGT-2, and potentially measure a GDGT-3+4 fraction. Additional sampling between 26cm and 46cm and between 50cm and 64 cm in this core could provide more information regarding how abrupt transitions in$\delta^{13}C$ are relative to the sedimentation changes that would appear to mark the transition into and out of an open marine setting from the initial position under the brine. Examination of trace metal concentrations, particularly Mn and Fe, through the core can help in better defining and characterizing changes in GDGTs in relation to a changing local environment. Scouring the literature for a better age model than the Flower et al. 2011 sedimentation rate estimations and the Ingram et al 2010 calculation that 100cm depth at Orca Basin is roughly 10ky BP would make it possible to constrain the time interval at which the brine pool recession occurred and may be linked to other known climate variations.

A quite specific note, it may be prudent to look back at peak structure for core OB depth 0.5cm. When OBI core depth 8.5cm was run for SWiM-IRMS, it produced an overloaded peak, which can drive the recorded isotopic measurement light in relation to the real value. The same phenomenon may have occurred in the uppermost sample from the other core, i.e. OB0.5cm explaining why it always seems to be at the bottom of the pile (Figure 6c). It may also prove interesting to try to sample the anoxic, chemocline, and oxic marginal Orca Basin cores analyzed in Hurtgen et al., 1999 to compare $\delta^{13}C_{GDGT}$ and $\Delta^{13}C_{GDGT}$ across the basin.

5.8.3: Assessing newly proposed $\Delta^{13}C_{GDGT}$ proxy systems

Validating my idea of using $\Delta^{13}C_{GDGT}$ to evaluate the heterogeneity of the community synthesizing GDGTs and as a paleo-$\delta^{13}C_{DIC}$ proxy will require a fair amount of leg work and lab time. Though the $\delta^{13}C_{GDGT}$ record as it currently exists supports the theory behind my suggested metrics of

$\Delta^{13}C_{1+2/0}$, $\Delta^{13}C_{Cren/0}$, and $\Delta^{13}C_0$, it will require a data set larger than n=10 featuring multiple localities where $\Delta^{13}C_{Cren/0}$ implies in-situ autotrophy to determine whether my $\delta^{13}C_{DIC}$ proxy holds up to the force of statistics. Best sections to next sample for compound specific GDGT SWiM-IRMS analyses would be places like the Red Sea samples vs. Gulf of Aden, Black Sea vs. Mediterranean Sea, the Mediterranean Sea vs. the Eastern Atlantic, and other known highly stratified water columns where rapid surface waters depletion of oxygen would allow for broad zones of alternative metabolisms, like manganese oxidation and iron reduction, to exist outside of the sediments. GDGT compound specific carbon isotopes from the Atlantic, Tethys, and Pacific reservoirs during Cretaceous OAEs could provide a basic measure as to whether these ratios can be proven to exist in the past.

Incorporating the relative abundances of *Thaumarchaeota* GDGTs predicted for 5°C waters based on [0/Cren] and [2/3] calibrations into isotope mass balance calculations may improve the quality of predictions for $\delta^{13}C$ of exogenous community, like the composition of my theoretical mixotrophic *Thaumarchaeota* + autotrophic others bottom water community model for the Orca Basin seawater/brine transition zone (Table 6; Equation 2). Of the variables involved in the paleo-$\delta^{13}C_{DIC}$ calculation, the fraction of GDGTs sourced from the general marine archaeal community as opposed to autotrophs at depth f_{MARINE} has proven the most difficult to accurately and precisely predict. Searching for statistical correlation between isotopic trends and the water column abundance of the lesser GDGTs largely excluded in this thesis (GDGT-3, -2, and cren isomer) may prove more useful in understanding mechanisms behind GDGT-based proxies, but will require processing of much greater amounts of sediment than sampled at Orca Basin, which could then degrade temporal resolution of sampling.

My initial naming suggestions are CAFS, or the crenarchaeol/GDGT-0 anomalous fractionation signal, for the autotrophy proxy based on $\Delta^{13}C_{Cren/0}$, L0P, or lighter GDGT-0 proxy, for the paleo-$\delta^{13}C_{DIC}$ measure, and 1-2STEP, or GDGT-1+2 similitude to tetraethers proxy for the $\Delta^{13}C_{1+2/0}$ index scaling the relative influence of local autotrophy and terrestrial runoff on the bulk sourcing of marine GDGTs. But I'm open to suggestions.

7: SUMMARY

Relative abundance of GDGTs through a 2300m Gulf of Mexico water column transect including the 200m hypersaline, anoxic Orca Basin brine at the bottom signal a benthic region of archaeal productivity; concentration spikes at depths coincident with reported zones of manganese oxidation (2174m) and iron reduction (2220m and 2242m) are characterized by different ratios of GDGT-0 to crenarchaeol. Core OB-0412-MC-0502C records a time window where the brine pool retreated from and then returned to cover the site; this allows for direct comparison of compound specific $\delta^{13}C_{GDGT}$ values and tetraether concentrations between depths, and ergo times, influenced by benthic autotrophy and those representative of oxic water column production statistically identical in $\delta^{13}C_{GDGT\text{-}0}$ and $\delta^{13}C_{Cren}$ to all previously measured Atlantic sites (Pearson et al. 2016). Spooling-wire microcombustion isotope ratio mass spectrometry (SWiM-IRMS) values and isotope mass balance calculations yield values of –19.3‰, –19.5‰, and –18.7‰ for Orca Basin open marine GDGT-0, -1+2, and crenarchaeol; –18.2‰, –18.6‰, and –18.4‰ for sediment deposited under brine pool conditions, thereby estimating an isotopic composition of –17.6‰, –18.2‰, and –18.2‰ for GDGTs produced in the seawater-brine transition ($\delta^{13}C_{TZ}$). If that pool of GDGT is treated as a two-end member mixture of archaea of the same composition as open marine values and purportedly everything non-*Thaumarchaeota*, the 'others' may have an isotopic composition ($\delta^{13}C_{Other}$) of around –16.0‰ for $\delta^{13}C_{GDGT\text{-}0}$, –15.9‰ for $\delta^{13}C_{GDGT\text{-}1+2}$, and –17.3‰ for $\delta^{13}C_{Cren}$.

Benthic, autotrophic synthesis of GDGTS is unlikely to be unique to the Orca Basin, and similar conditions may explain irregularities in other localities like the Red Sea. The $\delta^{13}C_{GDGT}$ record as it currently exists shows promise for of three $\Delta^{13}C_{GDGT}$ proxies that may represent heterogeneity in the source organisms producing GDGTs and reflect past carbon cycle states: (1) $\Delta^{13}C_{1+2/0}$ values <0.0‰ signal exogenous heterotrophic, likely terrestrial, production of GDGT-1 and GDGT-2 and values >0.0‰ imply exogenous productivity more autotrophic than the bulk marine community; (2) $\Delta^{13}C_{Cren/0}$ values less than 0.6‰ signal the presence of autotroph-synthesized GDGT-0, and (3) $\Delta^{13}C_0$ and $\Delta^{13}C_{Cren}$ between sites identified via $\Delta^{13}C_{Cren/0}$ and $\Delta^{13}C_{1+2/0}$ as open marine and autotroph-influenced can be used to construct an isotope mass balance system that may accurately reconstruct of paleo-$\delta^{13}C_{DIC}$ from $\delta^{13}C_{TZ,GDGT\text{-}0}$ or second step $\delta^{13}C_{Other,Cren}$ in absence of carbonates.

8: Acknowledgements

I would like to thank Courtney Warren for providing access to samples and data from the Orca Basin cruise and guidance throughout the course of the investigations; Felix Elling for access to his work on GDGT concentrations through the Orca Basin water column; Ann Pearson and the Harvard Department of Earth & Planetary Sciences' Laboratory for Molecular Biogeochemistry and Organic Geochemistry for welcoming this stranger into their midst, proving that real chemists do use burettes, and running the analyses which carried the greatest risk of long-term damaging home-made machines; Pincelli Hull for nudging me in all the right directions; and Mark Pagani for his patience (or at least will to more or less humor me) and for letting me play around with plastic in Cambridge for a summer, i.e. putting up with more than frankly he really should have. But I've learned that CO_2 sticks around for 400,000 years and to always beg forgiveness, so I'm a G&G success story. This senior project was funded by the Ezra Stiles Richter Summer Fellowship, the John E. Linck & Alanne Headland Linck Fellowship, the Yale College Dean's Research Fellowship in the Sciences, and the Yale Summer Environmental Fellowship. Additional support from the Karen Von Damm '77 Undergraduate Research Fellowship in Geology and Geophysics made it possible to present preliminary results at AGU 2015. A final thanks to all who have made KGL such a home to me the past four years.

9: REFERENCES

Antunes A., Ngugi D. K., and Stingl U. (2011). Microbiology of the Red Sea (and other) deep-sea anoxic brine lakes. *Environmental Microbiology Reports* **3**(4), 416-433.

Biddle J. F., Lipp J. S., Lever M. A., Lloyd K. G., Sorensen K. B., Anderson R., Fredricks H. F., Elvert M., Kelly T. J., Schrag D. P., Sogin M. L., Brenchley J. E., Teske A., House C. H., and Hinrichs K. U. (2006). Heterotrophic Archaea dominate sedimentary subsurface ecosystems off Peru. *Proceedings of the National Academy of Science USA* **103**, 3846-3851.

Brand, W. A., & Dobberstein, P. (1996). Isotope-ratio-monitoring liquid chromatography mass spectrometry (IRM-LCMS): first results from a moving wire interface system. *Isotopes in environmental and health studies*, *32*(2-3), 275-283.

Church M. J, Wai B., Karl D.M., and DeLong E.F. (2010). Abundances of crenarchaeol *amoA* genes and transcripts in the Pacific Ocean. *Environmental Microbiology* **12**, 679–688

Cordes E. E., Berrgquist D. C., and Fisher C. R. (2009). Macro-ecology of Gulf of Mexico cold seeps. *Annual Review of Marine Sciences* **1**, 143-168.

D'Hondt S., Arthur M.A. (1996). Late Cretaceous oceans and the cool tropic paradox. *Science* **271**(5257), 1838-1841.

Dirghangi S. S., Pagani M., Hren M. T., and Tipple B. J. (2013). Distribution of glycerol dialkyl glycerol tetraethers in soils from two environmental transects in the USA. *Organic Geochemistry* **59**, 49-60.

Eek K. M., Sessions A. L., and Lies D. P. (2007). Carbon-isotopic analysis of microbial cells sorted by flow cytometry. *Geobiology* **5**, 85-95.

Elling F. J., Könneke M., Lipp J. S., Becker K. W., Gagen E. J. and Hinrichs K. U. (2014). Effects of growth phase on the membrane lipid composition of the thaumarchaeon *Nitrosopumilus maritimus* and their implications for archaeal lipid distributions in the marine environment. *Geochimica et Cosmochimica Acta* **141**, 579-597.

Elling F. J., Könnecke M., Greve A., Mußmann M., and Hinrichs K.-U. (2015). Influence of temperature, pH, and salinity on membrane lipid composition and TEX_{86} of marine planktonic thaumarchaeal isolates. *Geochimica et Cosmochimica Acta* **171**, 238-255.

Erez J and Luz B. (1983). Experimental paleotemperature equation for planktonic foraminifera.

Geochimica et Cosmochimica Acta **47**(6), 1025–1031.

Flower B. P., Hastings D. W., and Randle N. J. (2011). Paired AMS ^{14}C dates on planktonic foraminifera from a Gulf of Mexico sediment core: An assessment of stratigraphic continuity. *Radiocarbon*, **53**, 377-344.

Francis C. A., Roberts K. J., Beman J. M., Santaro A. E., and Oakley B. B. (2005). Ubiquity and diversity of ammonia-oxidizing archaea in water columns and sediments of the ocean. *Proceedings of the National Academy of Sciences USA*, **102**, 1468-1688.

Greenwood D.R., Wing S.L. (1995). Eocene continental climates and latitudinal temperature gradients. *Geology* **23**(1), 1044-1048.

Ho S. L., Naafs B. D. A., and Lamy F. (2013). Alkenone Paleothermometry Based on the Haptophyte Algae. *The Encyclopedia of Quaternary Science*, 755-764.

Hoefs M. J. L., Schouten S., deLeeuw J. W., King L.L., Wakeham S.G., and Sinninghe Damsté J. S. (1997). Ether lipids of planktonic archaea in the marine water column. *Applied Environmental Microbiology* **63**, 3090-3095.

Huguet C., HOpmans E.C., Febo-Ayala W., Thompson D. H., Sinninghe Damsté J. S., and Schouten S. (2006). An improved method to determing the absolute abundance of glycerol dibiphytanyl glycerol tetraether lipids. *Organic Geochemistry* **37**, 1036-1041.

Hurtgen M. T., Lyons T. W., Ingall E. D., and Cruse A. M. (1999). Anomalous enrichments of iron monosulfide in euxinic marine sediments and the role of H_2S in iron sulfide transformations: examples from Effingham Inlet, Orca Basin, and the Black Sea. *American Journal of Science* **299**, 556-588.

Ingalls A. E., Shah S. R., Hansman R. L., Aluwihare L. I., Santos G. M., Druffel E. R. M., and Pearson A. (2006). Quantifying archaeal community autotrophy in the mesopelagic ocean using natural radiocarbon. *Proceedings of the Natl Academy of Sciences U.S.A.* **103**, 6442-6447.

Ingram W.C., Meyers S. R., Brunner C. A., and Martens C. S. (2010). Late Pleistocene-Holocene sedimentation surrounding an active seafloor gas-hydrate and cold-seep field on the Northern Gulf of Mexico Slope. *Marine Geology*, **278**(1-4), 43-53.

Jenkyns H.C., Forster A., Schouten S. and Sinninghe Damsté J. S. (2012). Warm Middle Jurassic-Early Cretaceous high-latitude sea-surface temperatures from the Southern Ocean. *Climate of the Past* **8**, 215-226.

Joye S. B., MacDonald I. R., Montoya J. P., and Peccini M. (2005). Geophysical and geochemical signatures of Gulf of Mexico seafloor brines. *Biogeosciences* **2**, 295-309.

Kim J. H., van der Meer J., Schouten S., Helmke P., Willmott V., Sangiorgi F., Koç N., Hopmans E. C., and Sinninghe Damsté J. S. (2010). New indices and calibrations derived from the distribution of crenarchaeol isoprenoid tetraether lipids: Implications for past sea surface temperature reconstructions. *Geochimica et Cosmochimica Acta* **74**(16), 4639-4654.

Kuypers M. M. M., Blokker P., Erbacher J., Kindel H., Pancost R. D., Schouten S. and Sinninghe Damsté J. S. (2001). Massive expansion of marine archaea during the mid-Cretaceous oceanic anoxic event. *Science* **293**, 92-94.

Lincoln S. A., Wai B., Eppley J. M., Church M. J., Simmons R. E., and DeLong E. F. (2014). Planktonic Euryarchaeota are a significant source of archaeal tetraether lipids in the ocean. *Proccedings of the National Academy of Sciences USA* **111**, 9858-9863.

Lunt D, Haywood A, Schmidt G, Salzmann U, Valdex P, and Dowsett H. (2009). Earth system sensitivity inferred from Pliocene modeling and data. *Nature Geoscience* **3**(1):60-64.

Mohr W., ant T., Sattin S. R., Bovee R. J., and Pearson A., (2014). Protein stable isotope fingerprinting: multidimensional protein chromatography coupled to stable isotope-ratio mass spectrometry. *Analytical Chemistry* **86**, 8514-8520.

Nelson D. M., Hu F. S. Mikucki J. A., Tian J., and Pearson A. (2007). Carbon-isotopic analysis of individual pollen grains from C_3 and C_4 grasses using a spooling-wire microcombustion interface. *Geochimica et Cosmochimica Acta* **71**(16), 4005-4014.

Ouverney C. C. and Fuhrman H. A. (2000). Marine planktonic Archaea take up amino acids. *Applied Environmental Microbiology*, **66**, 4829-4833.

Pearson A., Hurley S. J., Shah Walter S. R., Kusch S., Lichtin S., and Zhang Y. G. (2016). Stable carbon isotope ratios of intact GDGTs indicate heterogeneous sources to marine sediments. *Geochimica et Cosmochimica Acta* **181**, 18-35.

Peterse F., van der Meer J., Schouten S., Weijers J. W. H., Fierer N., Jackson R. B., Kim J-H, Sinninghe Damsté J. S. (2012). Revised calibration of the MBT-CBT paleotemperature proxy based on branched tetraether membrane lipids in surface soils. *Geochimica et Cosmochimica Acta* **96**, 215-229.

Pilcher R. S. and Blumstein R. D. (2007). Brine volume and salt dissolution rates in Orca Basin,

northeast Gulf of Mexico. *AAPG Bulletin* **91**(6), 823-833.

Qin W., Carlson L. T., Armbrust E. V., Devol A. H., Moffett J. W., Stahl D. A., and Ingalls A. E. (2015). Confounding effects of oxygen and temperature on the TEX_{86} signature of marine Thaumarchaeota. *Proceedings of the National Academy of Science USA* **112**, 10979-10984.

Santoro A. E., Casciotti K. L., and Francis C. A. (2010). Activity, abundance and diversity of nitrifying archaea and bacteria in the central California Current. *Environmental Microbiology* **12**, 1989-2006.

Sessions A. L., Sylvia S. P. and Hayes J. M. (2005). Moving-wire device for carbon isotopic analyses of nanogram quantities of nonvolatile organic carbon. *Analytical Chemistry* **77**, 6519-6527.

Schouten S., Hoefs M. J. L., Koopmans M. P., Bosch H. J., and Sinninghe Damsté J. S. (1998). Structural characterization, occurrence and fate of archaeal ether-bound acyclic and cyclic biphytanes and corresponding diol in sediments. *Organic Geochemistry* **29**, 1305-1319.

Schouten S., Hopmans E. C., Schefuß E., and Sinninghe Damsté J. S. (2002). Distributional variations in marine crenarchaeotal membrane lipids: A new organic proxy for reconstructing ancient sea water temperatures? *Earth and Planetary Sci. Letters* **204**, 265-274.

Schouten S., Hopmans E. C., and Sinninghe Damsté J. S. (2013). The organic geochemistry of glycerol dialkyl glycerol tetraether lipids: A review. *Organic Geochemistry* **54**, 19-61.

Shah, S. R., and Pearson A. (2007). Ultra-microscale (5-25 mu g C) analysis of individual lipids by C-14 AMS: assessment and correction for sample processing blanks. *Radiocarbon* **49**, 69-82.

Shah S. R., Mollenhauer G., Ohkouchi N., Eglinton T. I. and Pearson A. (2008). Origins of archaeal tetraether lipids in sediments: insights from radiocarbon analysis. *Geochimica et Cosmochimica Acta* **72**, 4577-4594.

Shah S. R., Joye S. B., Brandes J. A., and A. P. McNichol. (2013). Carbon isotopic evidence for microbial control of carbon supply to Orca Basin at the seawater-brine interface. *Biogeosciences* **10**, 3175-3183.

Shokes R. F., Trabant P. K., Presley B. J., and Reid D. F. (1977). Anoxic hypersaline basin in the Northern Gulf of Mexico. *Science* **196**, 1443-1446.

Smittenberg R. H., Baas M., Green M. J., Hopmans E. C., Schouten S., and Sinninghe Damsté J. S. (2005). Pre- and post- industrial environmental changes as revealed by the biogeochemical sedimentary record of Drammensfjord, Norway. *Marine Geology* **214**, 177-200.

Tierney J. E. (2014). Biomarker-Based Inferences of Past Climate: The TEX_{86} Paleotemperature Proxy. *Treatise on Geochemistry 2nd Edition* 379-393.

Tierney J. E., Mayes M. T., Meyer N., Johnson C., Swarzenski P. W., Cohen A. S. and Russell J. M. (2010). Late-twentieth-century warming in Lake Tanganyika unprecedented since AD 500. *Nature Geoscience* **3**, 422-425.

Trefry J. H., Presley B. J., Keeney-Kennicutt W. L., and Trocine R. P. (1984). Distribution and chemistry of manganese, iron, and suspended particulates in Orca Basin. *Geo-Marine Letters* **4**(2), 125-130.

Trommer G., Siccha M., van der Meer M. T. J., Schouten S., Sinninghe Damsté J. S., Schulz H., Hemleben C., and Kucera M. (2009). Distribution of Crenarchaeota tetraether membrane lipids in surface sediments from the Red Sea. *Organic Geochemistry* **40**(6), 724-731.

Van Cappellen P., Viollier E., Roychoudhury A., Clark L., Ingall E., Lowe K., and DiChristina T. (1998). Biogeochemical cycles of manganese and iron at the oxic-anoxic transition of a stratified marine basin (Orca Basin, Gulf of Mexico). *Environmental Science and Technology* **32**, 2931-2939.

Washburne, C. W. (1915). Chlorides in oil-field waters. *Transactions of the AIME* **48**(1), 687-694.

Wolfe J. A. (1993). A method of obtaining climatic parameters from leaf assemblages. *U.S. Geological Survey Bulletin* 2040: 1-71.

Xie S. T., Liu S. L., Schubotz F., Wakeham S. G., and Hinrichs K. U. (2014). Distribution of glycerol ether lipids in the oxygen minimum zone of the Eastern Tropical North Pacific Ocean. *Organic Geochemistry* **71**, 60-71.

Zhang Y. G., Zhang C. L., Liu X.-L., Li L., Hinrichs K.-U., and Noakes J. E. (2010). Methane Index: A tetraether archaeal lipid biomarker indicator fo detecting the instability of marine gas hydrates. *Earth and Planetary Science Letters* **307**, 525-534.

Zhang Y. G., Pagani M., and Wang Z. (2016). Ring Index: A new strategy to evaluate the integrity of TEX_{86} paleothermometry. *Paleoceanography* **31**(2), 220-232.

Zhuang, G., Elling F. J., Nigro L. M., Samarkin V., Joye S. B., Teske A., Hinrichs K. (2014). Ch 4: Multiple evidences for methylotrophic methanogenesis as the dominant methanogenic pathway in deep-sea hypersaline sediments. *Doctoral Dissertation, Methylotrophic methanogenesis and potential methylated substrates in marine sediment*, 89-129.